東京大学大学院新領域創成科学研究科
基盤科学研究系
先端エネルギー工学専攻

2004 年度修士論文

Measurement of Electric Field in a Flowing Plasma Using a Pockels Sensor

ポッケルスセンサによる フローイングプラズマ中の電場の測定

学籍番号　36213
氏 名　渡邉 将
指導教員　吉田 善章 教授

（2005 年 2 月 14 日提出）

Abstract

It is important to measure electric field structure in plasma in order to study the relaxation under the condition of a strong plasma flow and the confinement of fusion plasma and of non-neutral plasma. In particular, since transition to H-mode was discovered, the relation between internal electric field and confinement or anomalous transport has been researched. In Proto-RT, toroidal non-neutral plasma confinement system, generating radial electric field and strong toroidal flow is studied.

In these researches, it is important to measure electric field accurately. Although emissive Langmuir probe is known to be able to measure potential structure accurately, probe characteristics is too complicated and the effects of magnetic field or strong plasma flow have been under investigation. So Pockels sensor which is based on utilization of electro-optical effect and measures electric field directly is introduced.

Using this sensor, we measure electric field in variety of plasmas and compare to measurement result with emissive Langmuir probe. Two measurement results were almost the same in pure electron plasma. But generating strong plasma flow in neutral plasma, the electric field evaluated by emissive probe was smaller than that evaluated by Pockels sensor.

Moreover, influence emissive probe exerted by high speed plasma flow (greater than ion sound speed) is experimentally studied. When the plasma flow exceed ion sound velocity was generated, two results began to be different and emissive probe seemed over-estimate plasma potential.

Considering the experimental results that emissive probe error was observed at supersonic flow, this phenomenon may caused by ion acoustic shock wave (collisionless shock wave) and the potential structure around probe was calculated with one-dimensional model.

When Mach number exceeded 1.2, the potential hill arose in front of probe. This was why electrons emission started at the probe potential which was over the space potential and probe characteristics shifted in the direction of positive voltage.

Contents

Abstract **1**

Contents **3**

List of Figures **5**

List of Tables **7**

1 Introduction **9**

2 Proto-RT Device **11**

3 Electric Field Measurement **15**

3.1 Emissive Langmuir probe diagnostics 16

3.1.1 Langmuir probe (cold probe) characteristics 16

3.1.2 Emissive probe 17

3.2 Pockels sensor 20

3.2.1 Mach-Zehnder interferometer 20

3.2.2 Pockels sensor 21

4 Electric Field Structure in Plasmas **24**

4.1 Experimental setup 25

4.1.1 Proto-RT 25

4.1.2 Emissive probe 26

4.1.3 Pockels sensor 29

4.2 Electric field structures in plasmas 33

4.2.1 pure electron plasma 33

4.2.2 neutral plasma 37

4.2.3 electron injection 37

4.2.4 neutral plasma biased IC electrode 37

5 Effect of Fast Flow in Probe Measurement **48**
5.1 Experimental result 48
5.2 Calculation potential structure in ion acoustic wave 51

6 Summary **59**

A The Child-Langmuir Law **60**

B Pockels Effect **62**

Acknowledgments **65**

Bibliography **67**

Publications **68**

List of Figures

2.1 Photographic view of the Proto-RT 11
2.2 Schematic view of Proto-RT Device 12

3.1 I-V characteristic of single probe. 17
3.2 I-V characteristic of emissive probe. 18
3.3 Emission current-voltage characteristic and dI_{e0}/dV vs voltage 19
3.4 Comparison of characteristic of cold probe with that of hot probe 19
3.5 Schematic view of Mach-Zehnder interferometer. 20
3.6 Explanatory diagram of optical phase shift 23

4.1 The experimental setup of Proto-RT and the magnetic surface at dipole field. 24
4.2 The bird-eye view of Proto-RT. 25
4.3 Construction of and emissive Langmuir probe 26
4.4 Adjustable current regulator circuit 27
4.5 The emissive probe circuit. 28
4.6 Schematic diagram of Pockels sensor. 28
4.7 Photographic view of the Pockels sensor system. 29
4.8 Block diagram of Pockels sensor. 30
4.9 Schematic view of probe part 30
4.10 Configuration of Pockels sensor test 31
4.11 Plots of sensor output in variation of angles between Pockels sensor and electric field 31
4.12 Plots of sensor output at various intensity of electric field 32
4.13 Frequency characteristic of Pockels sensor (low frequency side) 32
4.14 Electron orbit injected at R=46cm 34
4.15 Radial potential profiles in pure electron plasma 34
4.16 Radial electric field profiles in pure electron plasma 35
4.17 Comparing measurement result of Pockels sensor and emissive probe in pure electron plasma 35
4.18 Radial potential profiles in neutral plasma 36

4.19 Radial electric field profiles in neutral plasma 36
4.20 Comparing measurement result of Pockels sensor and emissive probe in neutral plasma 38
4.21 Radial potential profiles in electron injection 38
4.22 Radial electric field profiles in electron injection 39
4.23 Comparing measurement result of Pockels sensor and emissive probe in electron injection 39
4.24 Potential structure measured with emissive probe in the variation of IC electrode bias voltage 41
4.25 The electric field profiles (1) 42
4.26 The electric field profiles (2) 43
4.27 The electric field profiles (3) 44
4.28 The comparison measurement results of electric field (1) 45
4.29 The comparison measurement results of electric field (2) 46
4.30 The comparison measurement of electric field (3) 47

5.1 Measurements of potential with emissive probe and Pockels sensor at R=40cm. 49
5.2 Radial electric field profile with Pockels sensor at V_{ic}=-40V to -60V. 49
5.3 Schematic of potential measurements with emissive probe and Pockels sensor. 50
5.4 Comparison of potential measurement with emissive probe (V_{pr}) and Pockels sensor (V_{se}) 50
5.5 Generation ion acoustic shock wave in front of probe. 51
5.6 Schematic of ion particle motion. We assume particles which can reach probe are absorbed and other particles are reflected. 52
5.7 Potential structure at $\tilde{M} = 1.5$ 54
5.8 Density of ions and electron and charge density profile at $\tilde{M} = 1.5$. 54
5.9 Ions and electrons distribution at $\tilde{M} = 1.5$. 55
5.10 Quasi-potential structure at $\tilde{M} = 1.5$ 56
5.11 Relation between $\hat{\phi}_{max}$ and Mach number 56
5.12 Schematic of I-V characteristic shift. 58

A.1 Schematic of the potential distribution among two planes 61

List of Tables

2.1 Principal parameter of Proto-RT 13
2.2 Typical parameter of neutral plasma at Proto-RT 14

3.1 Characteristics of electric field measurement. 16

B.1 Pockels coefficient of electro-optical crystals 64

Chapter 1

Introduction

In recent years, there is increasing interest in the role of the plasma flow in confinement. A plasma relaxation under the condition of strong plasma flow as fast as Alfvén velocity has studied by Mahajan-Yoshida[1, 2] and this state has the possibility for confinement of high β plasma observed at magnetosphere of Jupiter[3]. In this state, the condition is given by generalized Bernoulli's law balancing between plasma pressure and dynamical pressure. Strong plasma flow is generated by the electric field which is in a direction perpendicular to magnetic field line (radial direction in toroidal confinement). So this relaxation can be considered as confinement with electric field.

Generally, plasma is neutral seeing in broad perspective so there is scarcely existence of electric field in a plasma. It is necessary for generating electric field in a plasma to apply electric field from the outside or to turn into non-neutral condition. Non-neutral plasma has the self-electric field and there is the possibility to find characteristic which is degenerated in neutral condition.

The electric field has been considered as important parameter in plasma physics. A radial electric field may restrain ripple-loss at helical devices. In the tokamak researches, the transition from L-mode to H-mode was discovered in ASDEX [4] and the role of the electric field in H-mode has been studied theoretically[5, 6] and experimentally[7].

We have studied the relation between plasma confinements and internal electric field (plasma flow) in Proto-RT(Chapter 2). In this research, we often get electric field structures to calculate on measurement results of potential construction with emissive Langmuir probe. But there are some discussions the effects of magnetic field and strong plasma flow to probe, so it was desirable to measure electric fields with other methods.

For accurate measurement of electric field in plasma, we introduced Pockels sensor based on utilization of electro-optical effect. This sensor is able to measure electric field directly. In this study, we evaluate whether measurement with Pockels sensor is appropriate or not by comparing with measurement with emissive probe(Chapter 4). Moreover,

we examine exerting strong plasma flow on the emissive probe(Chapter 5).

Chapter 2

Proto-RT Device

Toroidal magnetic confinement has advantage in trapping high energy particles and multi-species with different charges simultaneously, because this system do not need a longitudinal electric field plugging open magnetic field line. Moreover, a large self-electric field in non-neutral plasma induces a strong toroidal flow by means of $\mathbf{E} \times \mathbf{B}$ drift and there is possibility of appearing new phenomena degenerating in neutral condition. In particular, an internal coil device has various advantages in studying interesting effect of flows in

Figure 2.1: Photographic view of the Proto-RT

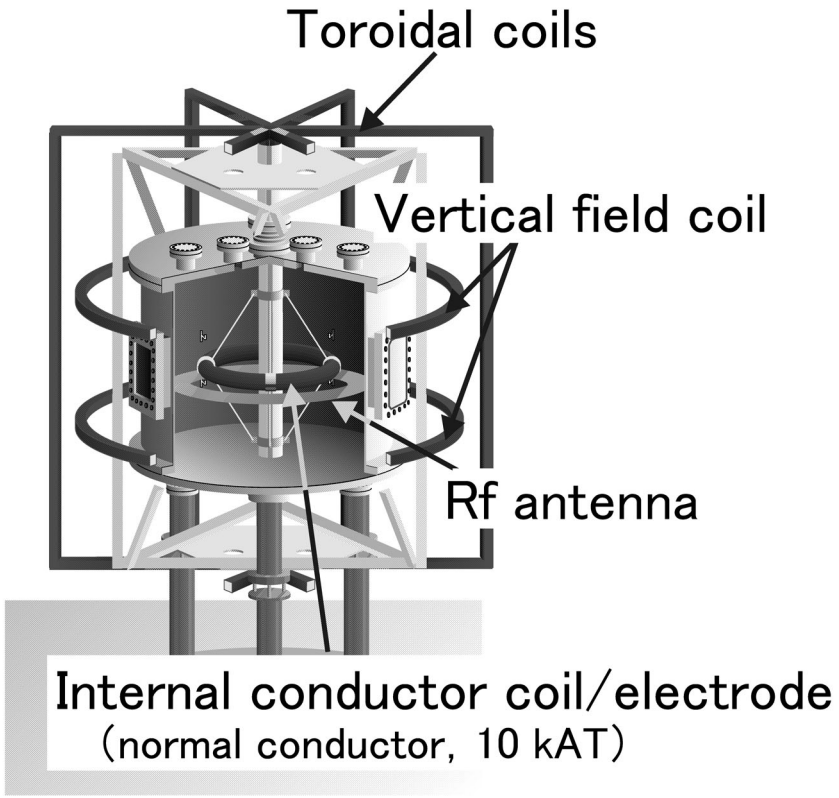

Figure 2.2: Schematic view of a toroidal non-neutral plasma confinement device Proto-RT.This device is able to generate various kind of magnetic field configuration with internal conductor, vertical field coils and toroidal field coils

plasmas.

The Proto-type Ring Trap (Proto-RT) device shown in Fig.2.1 and 2.2 is aiming to explore a new scheme of toroidal plasma confinement and generate radial electric field (toroidal flow) in plasma. This device can generate a variety of magnetic field configurations in combination of a dipole field, vertical field and toroidal field. The dipole magnetic field is generated by an internal ring conductor(IC). The machine parameters are summarized in Table 2.1. The vacuum vessel is 1.18 m in diameter and 0.90 m in height. This vessel is made of 1.0 cm thick stainless steel(SUS304) and contains a center stack with 11.4 cm diameter. The IC coil is suspended in the chamber by eight support rods which are stuck to the center stack. The major radius of the IC coil is 0.3 m and the minor radius is 4.3 cm. Inside the IC, there is a 175 turn copper wire with 3.2 mm diameter. The six toroidal field(TF) coils, which are 1.11 m in wide and 2.32 m in height, are passed through center stack. The pair of vertical field(VF) coils are located at outside of the chamber with a vertical interval of 0.6m. The magnetic field strength of each coil is 100 G(IC), 45 G(VF) and 120 G(TF) and DC power supply is 60 V, 60 A(IC), 120 V,

Table 2.1: Principal parameter of Proto-RT

Vacuum vessel (SUS304)	Inner diameter	1.18 m
	Height	0.90 m
	Thickness	1.0 cm
Internal ring (SUS304)	Major radius	30 cm
	Minor radius	4.3 cm
	Thickness	6 mm
	Coil wire	175 turn (copper)
	Wire diameter	3.2 mm
	DC power supply	60 V, 60 A
	Magnetic field strength	10-100 G
A pair of vertical coil	Diameter	180 cm
	Coil wire	175 turn in each (copper)
	Wire diameter	3.2 mm
	DC power supply	60 V, 30 A$\times$2
	Magnetic field strength	45 G
Six toroidal coils	Wide	111 cm
	Height	232 cm
	Coil board	10 turn in each (copper)
	Board thickness	1 mm
	DC power supply	50 V, 500A
	Magnetic field strength	120 G
Center Stack (SUS304)	Diameter	11.4 cm
Internal Conductor Electrode	Major radius	0.3m
	Minor radius	0.05m
	Material	SUS304
	Thickness	1.0mm
	Electrical insulation	$\sim$2 kV
Electron Gun	Cathode	LaB_6
	Acceleration voltage	2 kV

30A(VF) and 50 V, 500A(TF).

The IC coil's jacket has been installed the electrode which is made of 1 mm thick SUS304 stainless steel. This electrode can generate electric fields of radial direction.

An electron gun of LaB_6 cathode is inserted at $z = 0$. This gun can move along the radial direction and the angle of electron injection can also be freely aligned.

In Proto-RT, low density hydrogen neutral plasmas are generated by inductively-coupled 13.56 MHz RF discharge. The typical parameter of Proto-RT neutral plasma is

Table 2.2: Typical parameter of neutral plasma at Proto-RT

Electron density	$1.0 \times 10^{13} m^{-3}$
Electron temperature	10 eV
Ion temperature	1.0 eV
Neutral gas density	$8.8 \times 10^{18} m^{-3}$
Typical magnetic field strength	100 G
Debye length	$7.5 \times 10^{-3} m$
Ion sound velocity	$3.3 \times 10^{4} m/s$
Alfve'n velocity	$6.9 \times 10^{7} m/s$
Electron gyroradius	$7.6 \times 10^{-4} m$
Ion gyroradius	$1.0 \times 10^{-2} m$

summarized in Table. 2.2.

In the Proto-RT researches, we observe a long confinement time (> 0.1 sec, close to classical diffusion time) of a pure electron plasma with control of the electrostatic potential (internal conductor voltage V_{ic}). Then the equi-potential surfaces well accord with the magnetic surface[8].

In neutral plasmas, we may produce a strong flow with applying the potential control[9]. In the Proto-RT plasmas, electromagnetic forces and neutral collisional effects are dominant in determining the motion of charged particle. Suppose to only pure poloidal magnetic fields, the radial electric field yields toroidal rotation of plasmas. When we neglect the inertia of particles, the equation of motion for ions and electrons in steady state is approximately written by

$$q_k n_k \left(\mathbf{E} + \mathbf{v_k} \times \mathbf{B}\right) - m_k n_k \nu_{nk} \mathbf{v_k} = 0 \tag{2.1}$$

where q, n, m are charge, density and mass of charged particles , ν is the collision frequency between neutral particles and charged particles and suffix $k = i, e$ indicates ion and electron. (2.1) leads the velocity perpendicular to the magnetic field

$$\mathbf{v_k} = \frac{q_k \nu_{nk} \mathbf{E}}{m_k {\omega_{ck}}^2} + \frac{\mathbf{E} \times \mathbf{B}}{B^2} \tag{2.2}$$

where ω_{ck} is the cyclotron frequency. The first term corresponds to the radial motion of charged particles across the magnetic field lines and the second term is the toroidal field speed. The internal electric field ($E_r \sim 10^3 V/m$) drives strong plasma flow of order $10^5 m/s$ by $\mathbf{E} \times \mathbf{B}$ drift and this flow speed is higher than the ion sound speed.

When electrons are injected into neutral plasmas, the plasma potential falls down to nearly zero (chamber voltage). But a negative potential is not able to be achieved.

Chapter 3

Electric Field Measurement

There are various methods to measure an electric field. Since H-mode was discovered and it was indicated that the radial electric field is closely connected with improved confinement, electric field measurements with enough spatial and time resolution have been needed. Also, an electric field in sheath and presheath regions plays essential roles in plasma processing of materials so variety of electric field measurement have been developed.

The methods which are used in recent fusion plasma experiments are measuring plasma flow. Generating steady electric field needs the force to keep the distribution difference between ions and electrons. Consequently, an electric field in plasma is determined by equation of motion

$$m_i n_i \frac{\partial \mathbf{V}}{\partial t} + m_i n_i \mathbf{V} \cdot \nabla \mathbf{V} = -\nabla p - \nabla \Pi + \rho \mathbf{E} + \mathbf{j} \times \mathbf{B} + \mathbf{F} \tag{3.1}$$

where $\mathbf{V}$ is plasma flow velocity, m_i is ion mass, n_i is ion density, ρ is charge density, $\mathbf{F}$ is external force, p and Π are diagonal term and non-diagonal term of pressure tensor respectively. When bulk ion flow velocity is measured, pressure gradient term is negligible and (3.1) is rewritten by

$$\mathbf{V} = \frac{\mathbf{E} \times \mathbf{B}}{B^2} + \frac{\nabla p \times \mathbf{B}}{n \rho B^2}. \tag{3.2}$$

The technique which have been used commonly is based on the Doppler shift measurement of plasma spectra. For instance, there are ultraviolet/visible spectroscopy[10] and charge-exchange recombination method[11].

Space charge electric fields can be derived from local measurement of the plasma potential ($\mathbf{E_{sc}} = -\nabla\phi$, ϕ is the plasma potential) using Langmuir probe, emissive probe and heavy ion beam probe method.

There are the methods measuring electric field directly. For example, laser Stark spectroscopy has been used and laser-induced fluorescence-dip spectroscopy which has

Table 3.1: Characteristics of electric field measurement.

measurement method	frequency	measurable area	material of sensor
Laser-induced fluorescence-dip spectroscopy[12]		0.6∼30 kV/m	noncontact
Heavy ion beam probe		kV∼	noncontact
Dipoler double probe[13]	DC∼20MHz	1mV/m∼	metal
Piezo·inverse piezo effect[14]	constant	10 V/m∼	crystal
Pockels effect	6∼2 GHz	5 V/m∼	crystal

superior ability in sensitivity to Stark spectroscopy has been developed. This spectroscopy is based on optical double resonance of H or Ar atoms. The method to measure electrically is dipole double probe method. This method is able to measure not only

In this experiment, we used emissive probe measurement and introduced Pockels sensor measurement for the first time.

3.1 Emissive Langmuir probe diagnostics

3.1.1 Langmuir probe (cold probe) characteristics

Langmuir probe (electrostatic probe) is the one of the fundamental techniques for measuring the properties of plasmas. In many cases probe consists of small metallic tip and inserted into plasma. We measure probe current(I_p) varying biased voltage(V_p) and estimate plasma parameter(electron density, temperature etc) by means of current-voltage(I-V) characteristics. This method is one of the most popular diagnostics and capable of time resolution and spatial resolution. But the perturbation of probe to plasmas is relatively large and the use of probe is restricted only low temperature and low density plasmas.

Fig.3.1 shows the typical I-V characteristics of single probe. At the space potential (V_s), ions and electrons can come into a probe. In an unperturbed plasma, elementary gas-kinetic theory gives particle flux density Γ as follows

$$\Gamma = \frac{1}{4} n \bar{v} \tag{3.3}$$

where n is plasma density and $\bar{v}$ is the mean particle speed. The current (I) is given by

$$I = q\Gamma \tag{3.4}$$

where q is electric charge. Suppose that a thermal plasma of comparable electron and ion temperatures is considered, the ion thermal speed will be much smaller than the

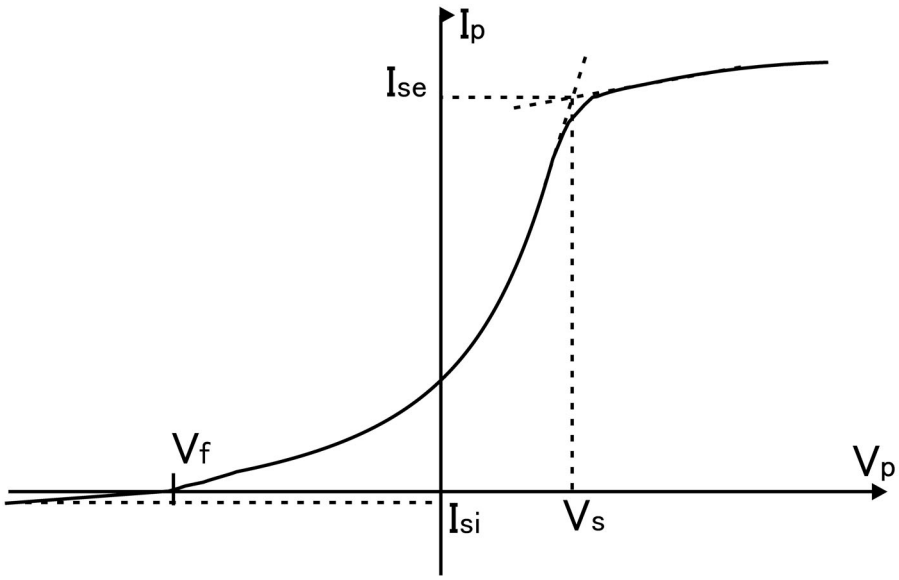

Figure 3.1: I-V characteristic of single probe.

electron thermal velocity. When V_p is above V_s, the electron current is dominant. If V_p is increased moreover, the sheath is generated around the probe so the electron current cannot increase any further (electron saturation current:I_{se}). Then I_p is shown as follows

$$I_p\,(= I_{se}) = -\frac{nev_{the}}{4} \qquad (V_p \geq V_s) \tag{3.5}$$

where v_{the} is electron thermal velocity. When V_p <V_s, the low energy electrons are repelled and ions flow to a probe freely. The V_p at which the ion current is equal to the electron current is the floating potential V_f.

3.1.2 Emissive probe

Emissive probe is the Langmuir probe specialized in potential measurement. A tip of emissive probe is filament and heated in order to emit heat electron. To measure with emissive probe depends on the basic principle that heat electrons emitted from tip biased above plasma potential is reflected back to the probe and only electrons below plasma potential can enter plasma.

We consider probe temperature as T_w, emissive probe emits heat electrons which energy is about kT_w of constant current I_{e0}. When probe voltage is negative rather than plasma space potential, the heat electrons from probe is discharged into plasma. Assuming that shape of electrode is cylindrical probe and space charge limit is neglected,

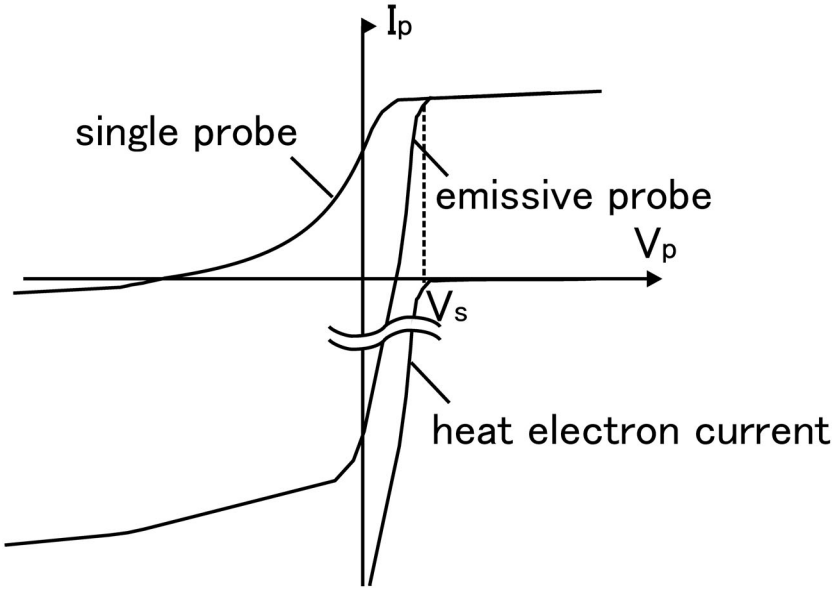

Figure 3.2: I-V characteristic of emissive probe.

the emission current is given by Richardson-Dushman's formula,

$$j_{ep}^{-} = AT_w^2 \exp\left[-\frac{e\phi_w}{kT_w}\right] \tag{3.6}$$

where A is Dushman's constant, T_w is the temperature of the probe and ϕ_w is the work function of the material surface of the probe. So probe current I_{ep} owing to heat electrons can be written by

$$\begin{aligned} I_{ep} &\simeq -I_{e0}\left[-\frac{e\,(V_p - V_s)}{kT_w}\right]\left[\frac{e\,(V_p - V_s)}{kT_e} + 1\right]^{1/2} && (V_p \geq V_s) \\ I_{ep} &= -I_{e0} && (V_p \leq V_s). \end{aligned} \tag{3.7}$$

Additionally, probe current I_p is added to plasma electron current and given by

$$\begin{aligned} I_{ep} &\simeq A_p|j_0|\left[\frac{e\,(V_p - V_s)}{kT_e} + 1\right]^{1/2} - I_{e0}\left[-\frac{e\,(V_p - V_s)}{kT_w}\right]\left[\frac{e\,(V_p - V_s)}{kT_e} + 1\right]^{1/2} && (V_p \geq V_s) \\ I_{ep} &\simeq A_p|j_0|\left[\frac{e\,(V_p - V_s)}{kT_e}\right]^{1/2} - I_{e0} && (V_p \leq V_s). \end{aligned} \tag{3.8}$$

Fig.3.2 shows I-V characteristic of emissive probe near space potential. Ordinarily, contribution to probe current from heat electrons changes dramatically at $V_p \simeq 0$, so this probe can measure accurately in principle.

This probe have been used to measure the plasma potential by several techniques in a variety of plasmas. Typical techniques are to measure the voltage at which the Langmuir probe (cold probe) and emissive probe (hot probe) I-V characteristics separate[15], inflection point method[16, 17] and floating potential method [18].

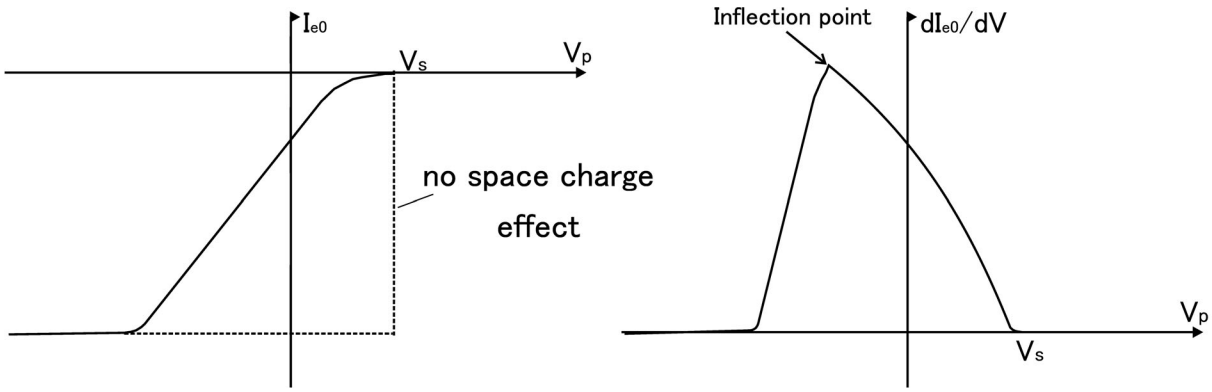

Figure 3.3: Emission current-voltage characteristic(left side) and dI_{e0}/dV vs voltage(right side)

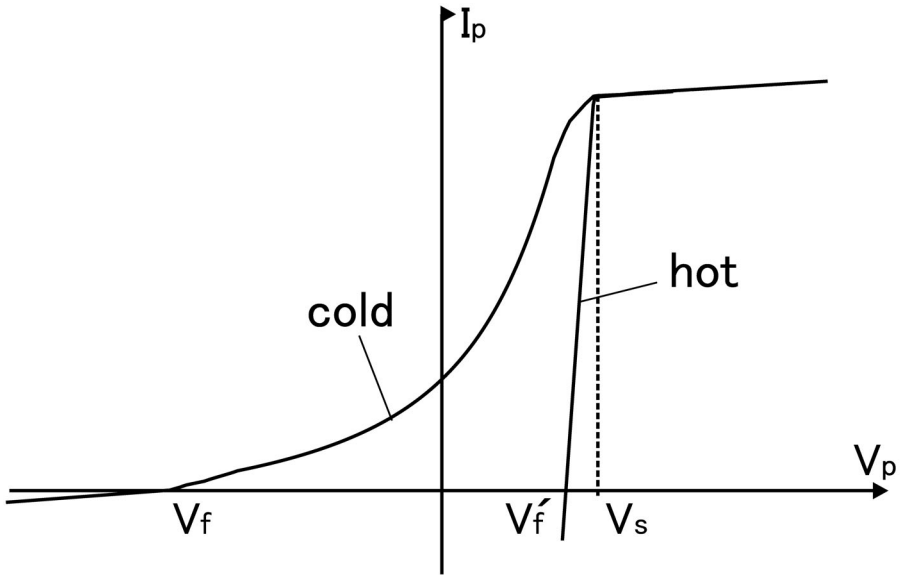

Figure 3.4: Comparison of characteristic of cold probe with that of hot probe. The floating potential of hot probe is nearer to space potential than that of cold probe.

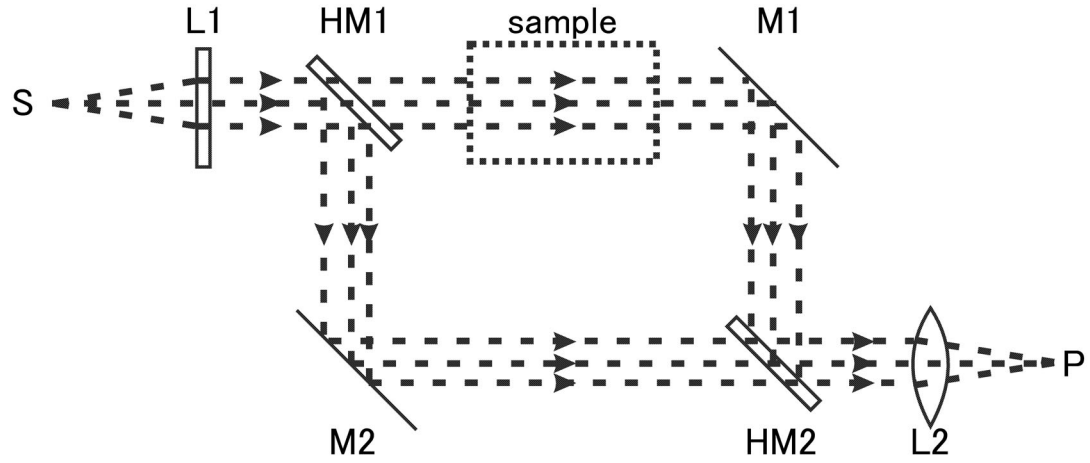

Figure 3.5: Schematic view of Mach-Zehnder interferometer.

Separation point method is the simplest techniques. This method is measuring cold probe and hot probe characteristics and considering the voltage at which two characteristics separate as space potential. This method is useful for stationary and relatively low density plasma.

Inflection point method is paying notice to emission current given by cold probe and hot probe characteristics. If the space charge effect is neglected, I_{e0}-V characteristic resembles a step function (fig.3.4). The space charge effect is considered, the inflection point of I_{e0}-V characteristic determined by the peak of dI_{e0}/dV gives the plasma space potential. The gap between potential measured with this method from actual plasma potential is getting larger when T_w increases[19].

Floating potential method is to measure with high impedance in order to get the potential where $I_p \sim 0$. This method needs sufficient electron emission near space charge limitation. For strong emission, V_f shifts near V_s (V_f').

3.2 Pockels sensor

3.2.1 Mach-Zehnder interferometer

The Mach-Zehnder interferometer, which was developed by L.Mach and L.Zehnder almost at the same time in 1891, is a type of the double-beam interferometer and has been used to determine the phase shift caused by a sample which is to be placed in one of two light paths from a coherent light source. This interferometer has superior versatility and elasticity.

Fig.3.5 shows schematic of Mach-Zehnder interferometer. This interferometer consists of lens, mirrors and half mirrors. The light from light source changes parallel light at collimator lens (L1) and is divided transmitted light from reflected light at half-mirror (HM1). Reflected light is reflected at mirror (M1) and passes through HM2 and L2. At the same time, transmitted light is reflected at M2 and HM2 and passes through L2.

Without a sample there is no phase difference for the two paths. If a sample in placed in placed in one light path, two light will interfere and there will be phase difference according to optical path difference generated by sample.

3.2.2 Pockels sensor

Pockels sensor is a instrument measuring electric field using Pockels effect. Pockels effect is one of the electro-optical effects and has been used to measure a high voltage. When an electric field is applied to Pockels crystal, birefringence which is proportional to the electric field occurs. The difference of refractive indices Δn between two polarized electromagnetic radiations in the crystal is given as the first order function of E as follows

$$\Delta n = \Delta n_0 + \Delta a E \tag{3.9}$$

where Δn_0 and $\Delta a E$ term represent the natural birefringence and the Pockels effect respectively. Δa can be written as

$$\Delta a = {n_0}^3 \gamma_p \tag{3.10}$$

where n_0 is the normal refractive index and γ_p is the Pockels coefficient of the crystal. Here, we consider Mach-Zehnder interferometer on Pockels crystal. When the light wave written as

$$E_{int} = E_0 \cos(\omega t) \tag{3.11}$$

enters this crystal, a light passes through this interferometer separates two lights as follows

$$E_1 = \frac{E_0}{2} \cos(\omega t - \phi_1) \tag{3.12}$$

$$E_2 = \frac{E_0}{2} \cos(\omega t - \phi_2) \tag{3.13}$$

where ϕ_1, ϕ_2 are phase differences during light passing through the interferometer. When the electric field E applies the crystal, the birefringence causes an optical path difference between two light paths. Assuming Δn is constant during there light passes through it, the phase shift $\Delta\theta$ is given by

$$\Delta\theta = \frac{2\pi l}{\lambda} \Delta n \tag{3.14}$$

where λ is the wave length of the light and l is the length of the crystal along the light path. Therefore synthesis light is represented by following expression

$$E_{out} = E_0 \cos\left(\Delta\theta - \frac{\phi_1 - \phi_2}{2}\right) \cos\left(\omega t - \frac{\phi_1 + \phi_2}{2}\right). \tag{3.15}$$

Considering no time dependence and

$$\psi = \frac{\phi_1 - \phi_2}{2}, \tag{3.16}$$

the output light intensity is given by

$$I_{out} = \frac{{E_0}^2}{2} \left\{1 + \cos\left(\Delta\theta + \psi\right)\right\}. \tag{3.17}$$

Here, ψ, where is called bias angle, is represented by path difference between two paths when an electric field doesn't apply to the crystal. When we consider as $\psi = \frac{\pi}{2}$ and $\Delta\theta \sim 0$, (3.17) is rewritten by

$$I_{out} = \frac{I_{in}}{2} \left\{1 - \Delta\theta\right\} \tag{3.18}$$

where $I_{in} = {E_0}^2$. So the output intensity is as proportional to an applied electric field intensity as can be expected from (3.18). Fig.3.6 shows an simplistic explanatory diagram of optical phase shift (adjusting I_{out}=0 at $E = 0$).

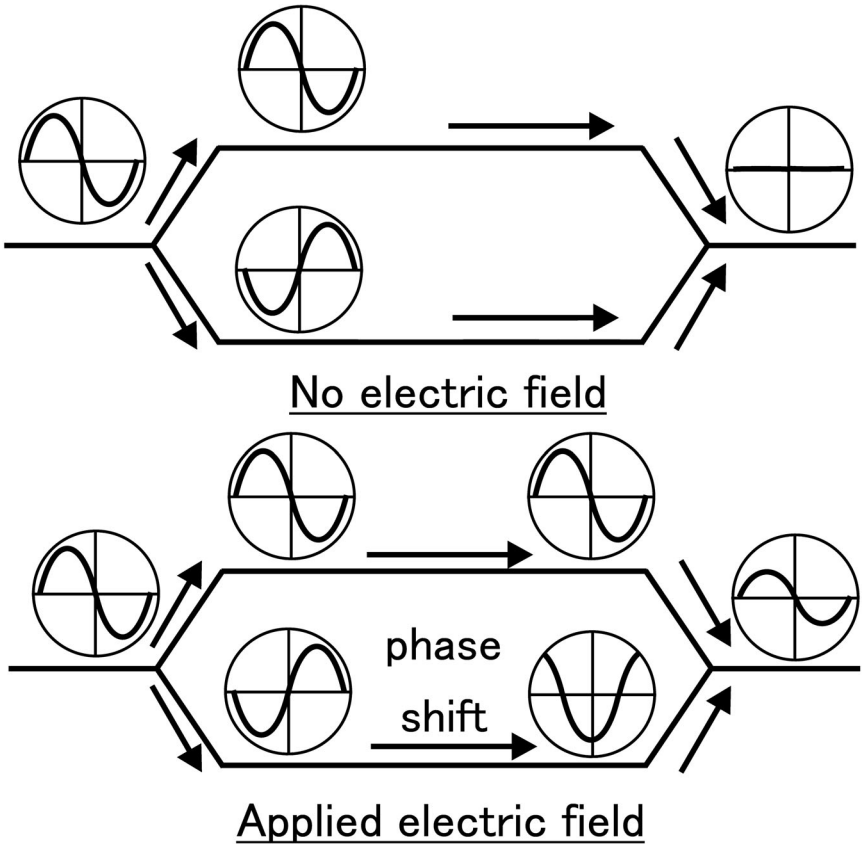

Figure 3.6: Explanatory diagram of optical phase shift. The optical intensity is zero (upper side). However, if the refractive indices of the two waveguides differ, the optical phases of the respective lights are shifted after merging. This increases the optical intensity.

Chapter 4

Electric Field Structure in Plasmas

Electric field structures in plasmas were measured with emissive probe and Pockels sensor simultaneously in Proto-RT and two measurement results were compared. The goal of this study is to determine whether Pockels sensor measurement be appropriate or not. The potentials of three types plasmas(pure electron plasma, weak flow neutral plasma and strong flow neutral plasma) and neutral plasmas injected electrons with electron gun were measured. In emissive probe measurement, we considered floating potentials of high impedance probe as plasma potentials.

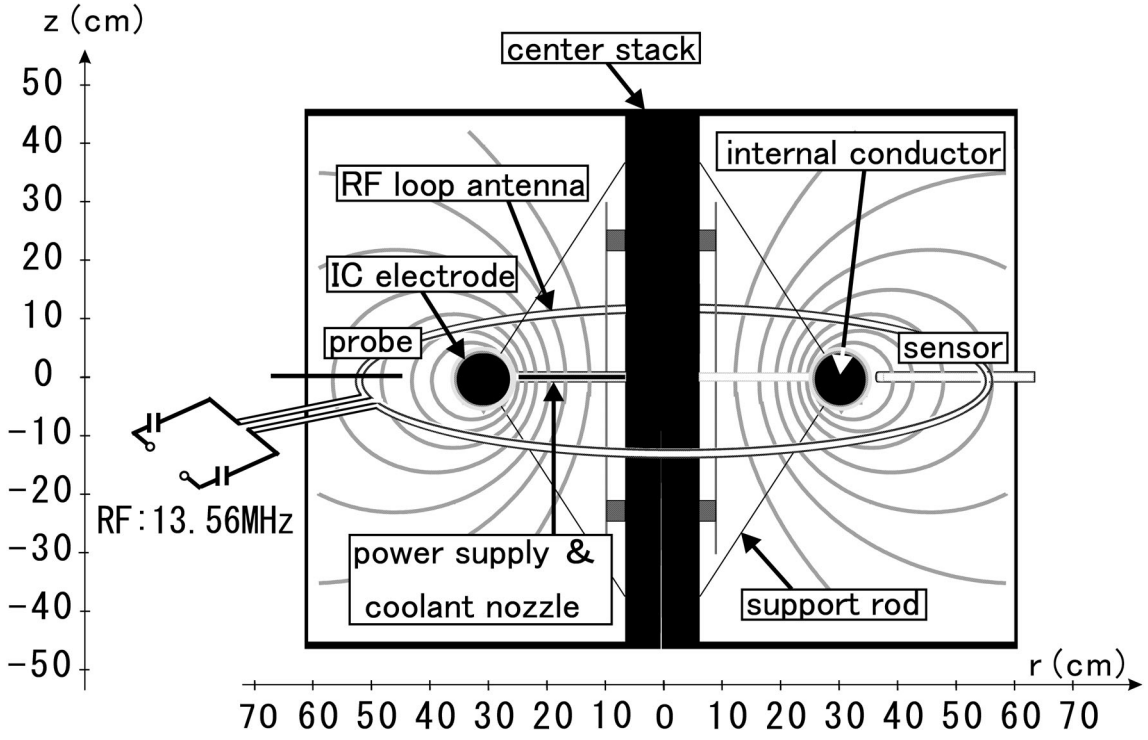

Figure 4.1: The experimental setup of Proto-RT and the magnetic surface at dipole field.

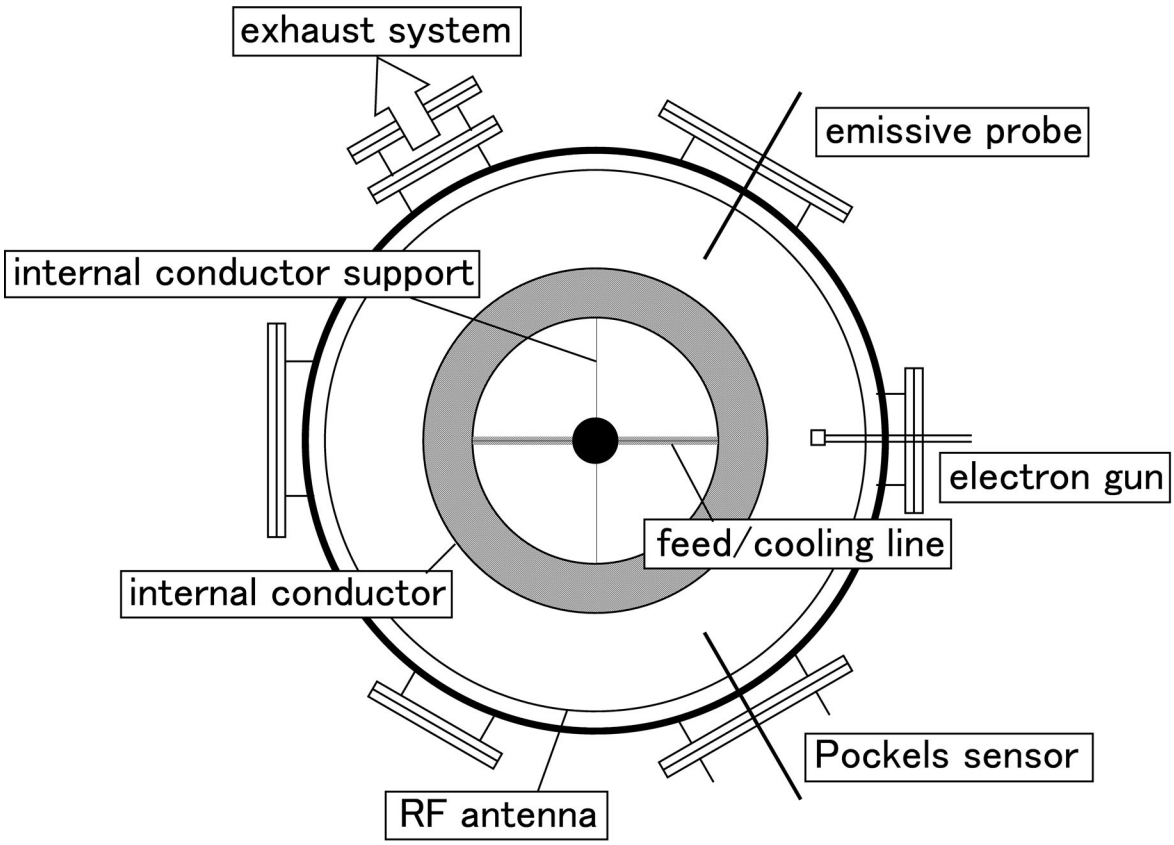

Figure 4.2: The bird-eye view of Proto-RT.

4.1 Experimental setup

All experiments were carried out at Proto-RT which is able to confine both non-neutral plasma and neutral plasma. When we generated toroidal plasma flow, we used IC electrode or electron injection. But an internal electric field product with electron injection hardly succeeded. Measuring a radial electric field profile, we used emissive probe and Pockels sensor.

4.1.1 Proto-RT

Fig.4.1, 4.2 shows the experimental setup of Proto-RT and the magnetic surface at dipole field. We experimented with the dipole magnetic field generated by 7.0 kAturn IC coil current.

By inductively-coupled 13.56MHz RF discharge with loop antenna, we produced neutral plasmas. Hydrogen pressure was 4.0×10^{-4} Torr.

In pure electron plasma experiments, we removed roop antenna. Base pressure was 4.0×10^{-7} Torr by a turbomolecular pump.

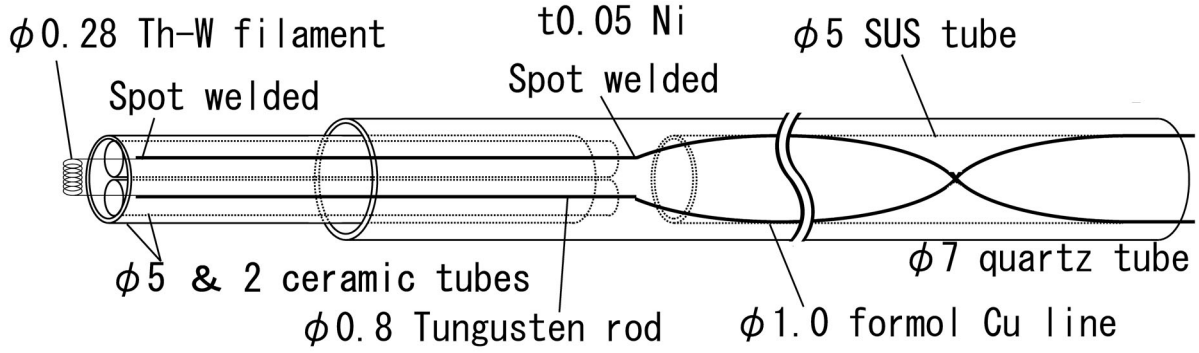

Figure 4.3: Construction of and emissive Langmuir probe. Thoria-tungsten is wound around ϕ 0.5 wire for 10 turns.

We measured potential structure with emissive probe between 37cm and 50cm and electric field structure with Pockels sensor between 38cm and 50cm.

4.1.2 Emissive probe

Construction of emissive probe

For radial potential measurement at $z = 0$, we used emissive Langmuir probe. The construction of probe is shown by Fig.4.3. We used Thoria-tungsten wire for the tip of this probe. ϕ 0.28 wire is wound around ϕ 0.5 wire for 10 turns. The tip surface was $4.4\times10^{-6}m^2$. This tip wire was spot welded to Tungsten ϕ 0.8 rods. To protect Tungsten rods against electron beam current, we covered with doubly ceramic tubes(two ϕ 2 tubes inside ϕ 5 tube).

Electric circuit of adjustable current regulator

For heating an emissive probe tip, we used adjustable current regulator. The required current for the emission from ϕ 0.28 tungsten wire is about 4A.

Figure.4.4 shows adjustable current regulator circuit. The LM338 series of adjustable 3-terminal positive voltage regulator is capable of supplying in excess of 5A over a 1.2V to 32V output range. Using the LM 338, this adjustable current regulator can supplying current up to 5A. The Power source of this circuit employs 12V battery and the reference voltage is -9V which is supplied from dry battery.

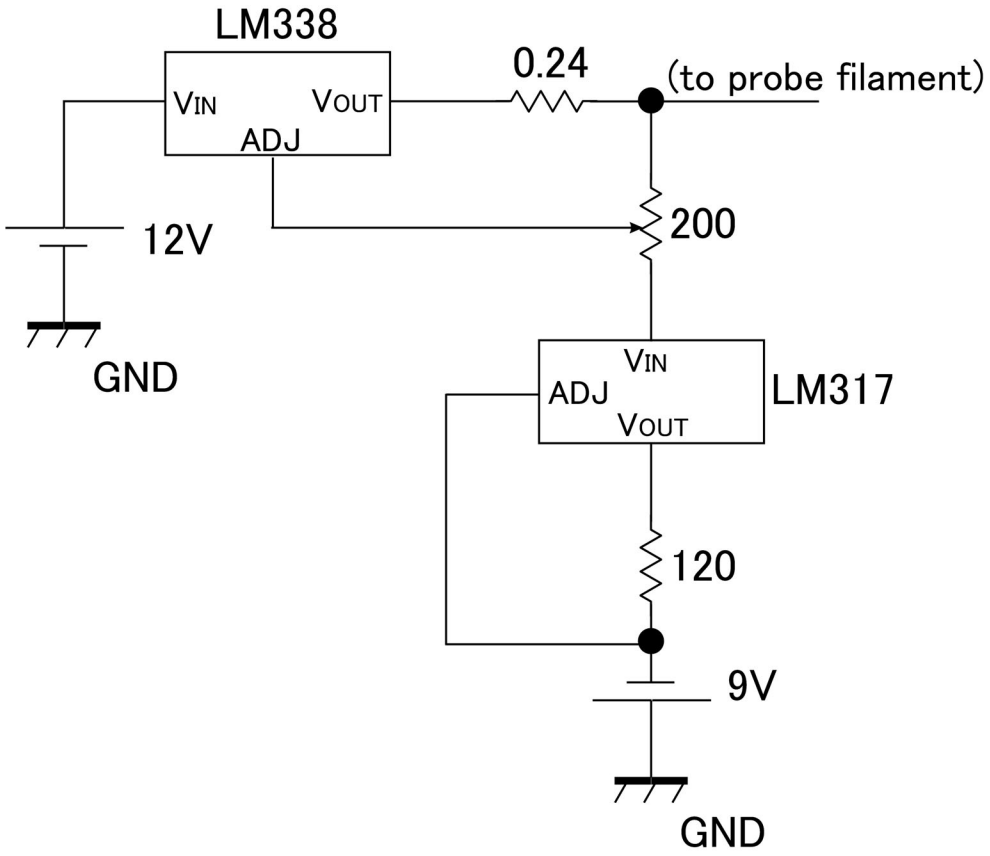

Figure 4.4: Adjustable current regulator. This regulator is capable of supplying current up to 5 A.

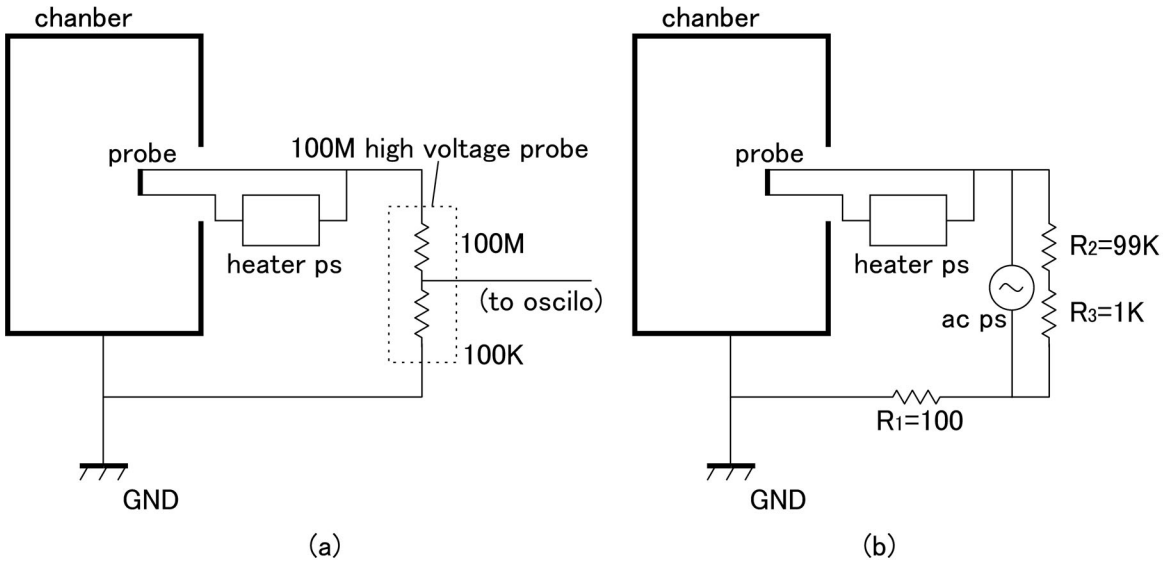

Figure 4.5: The emissive probe circuit. (a) For the floating potential measurement. (b) For the current-voltage measurement. The probe characteristics are obtained in sweeping of the ac power source.

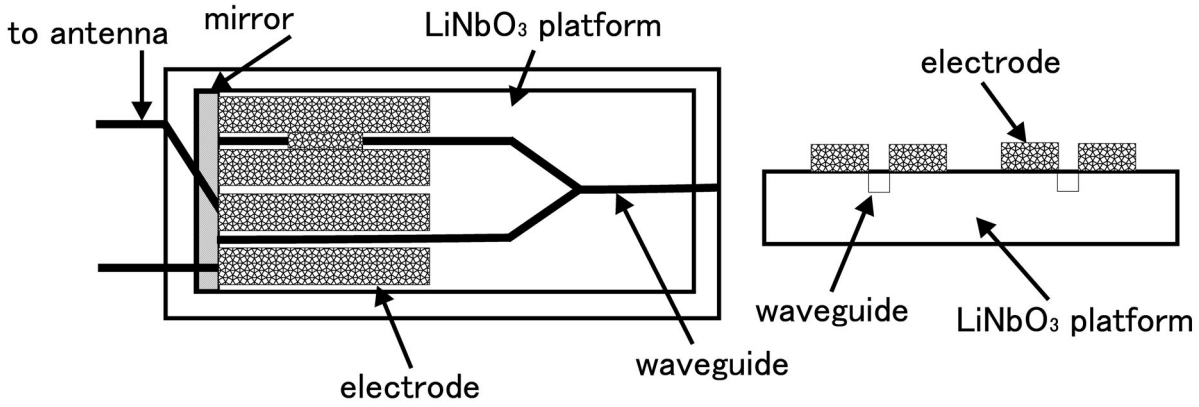

Figure 4.6: Schematic diagram of Pockels sensor. A Mach-Zehnder interferometer is produced on $LiNbO_3$ platform.

Emissive probe measurement circuit

Fig.4.5(a) shows measurement of emissive floating potential. By using the high impedance probe, we can measure V_f. Because probe current is given by

$$I_p = \frac{V_p}{R} \tag{4.1}$$

so when R is large enough, I_p is approximately zero. If the probe tip emits electrons sufficiently, the V_f will approach to the V_s. We employed high voltage probe of 100MΩ.

Fig.4.5(b) is a probe circuit of the current-voltage measurement (basic circuit for Langmuir probe diagnostics). For the measurement of I-V characteristics, I_p is given by R_1 (small resistor in order to prevent current loss) and V_p is given by R_3. R_2 is larger resistor than R_3 for voltage dividing. The probe characteristics is obtained in sweeping of the ac power source (frequency is 1Hz).

4.1.3 Pockels sensor

We use the electric field sensor developed by the Toyota Central Research and Development Laboratories, Inc[20]. This sensor employs $LiNbO_3$ as Pockels crystal and is integrated retro-reflective structure based on the Mach-Zehnder interferometer (Fig.4.6). It consists of a Y-junction optical wave guide formed by titanium diffusion.

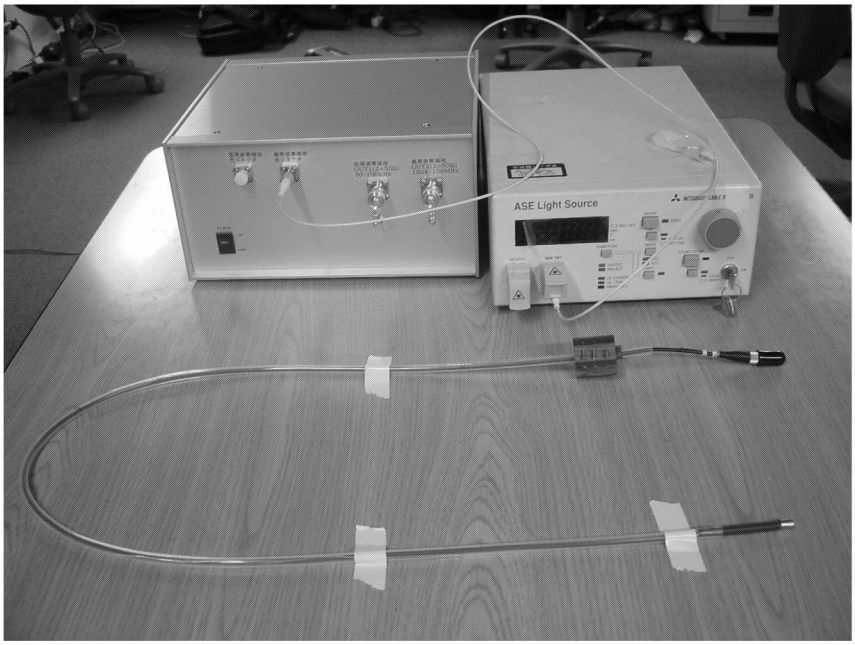

Figure 4.7: Photographic view of the Pockels sensor system.

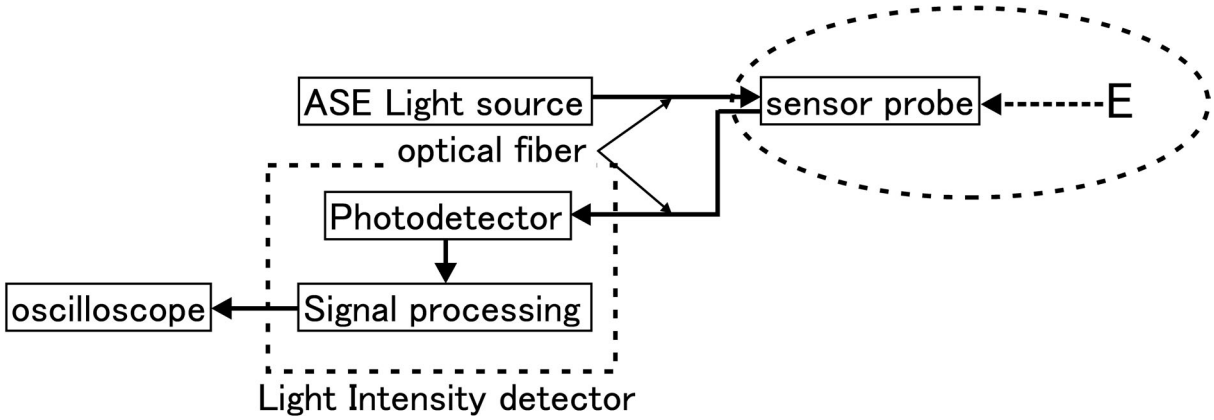

Figure 4.8: Block diagram of Pockels sensor.

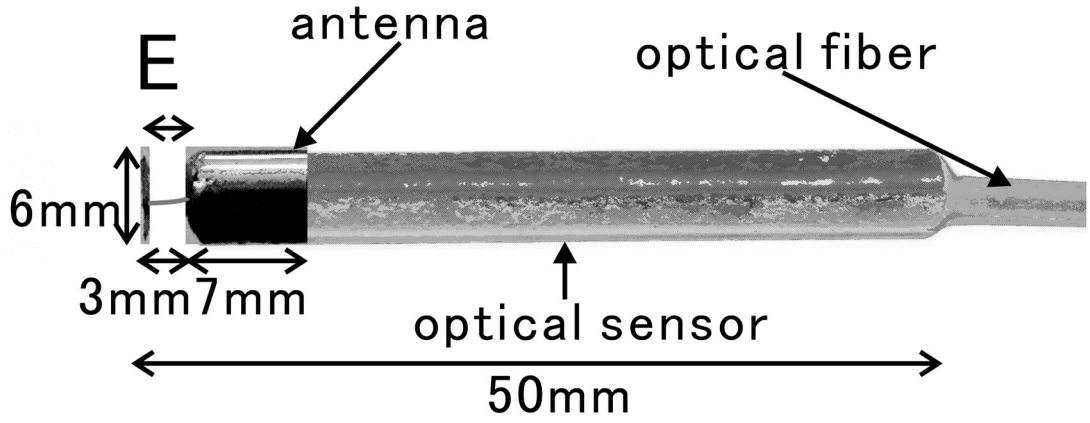

Figure 4.9: Schematic view of probe part. The tip antenna can be changed.

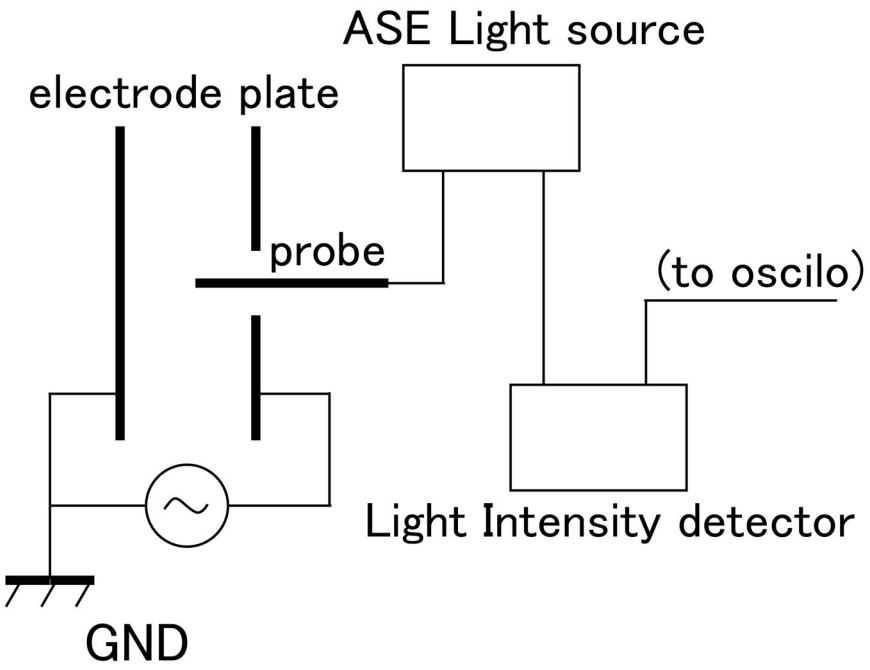

Figure 4.10: Configuration of Pockels sensor test. The voltage between electrode plates is measured by high impedance probe.

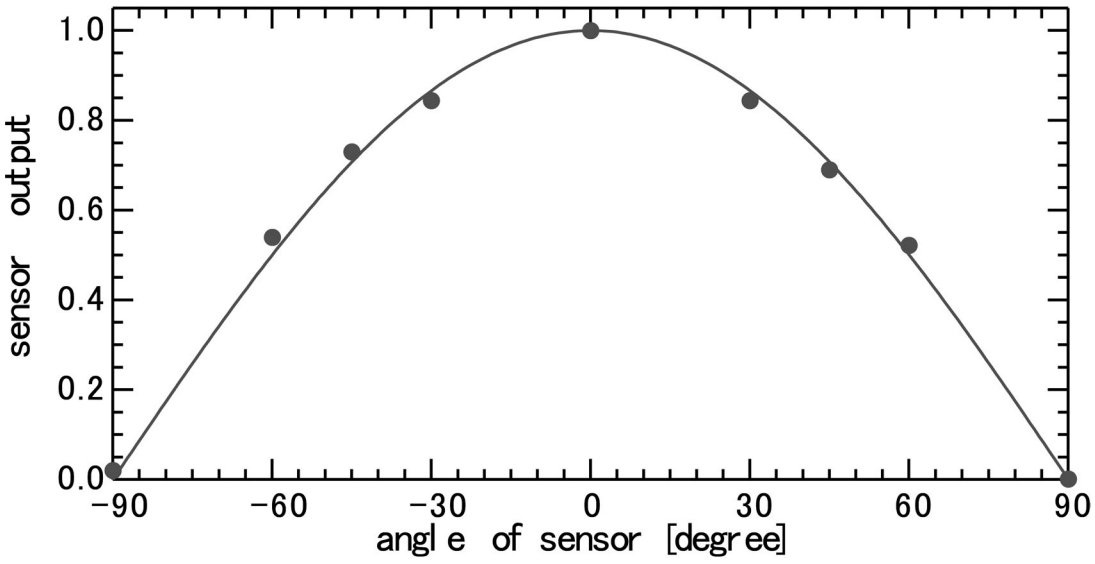

Figure 4.11: Plots of sensor output normalized by maximum at various angles between Pockels sensor and electric field. This character is dependent of tip antennas.

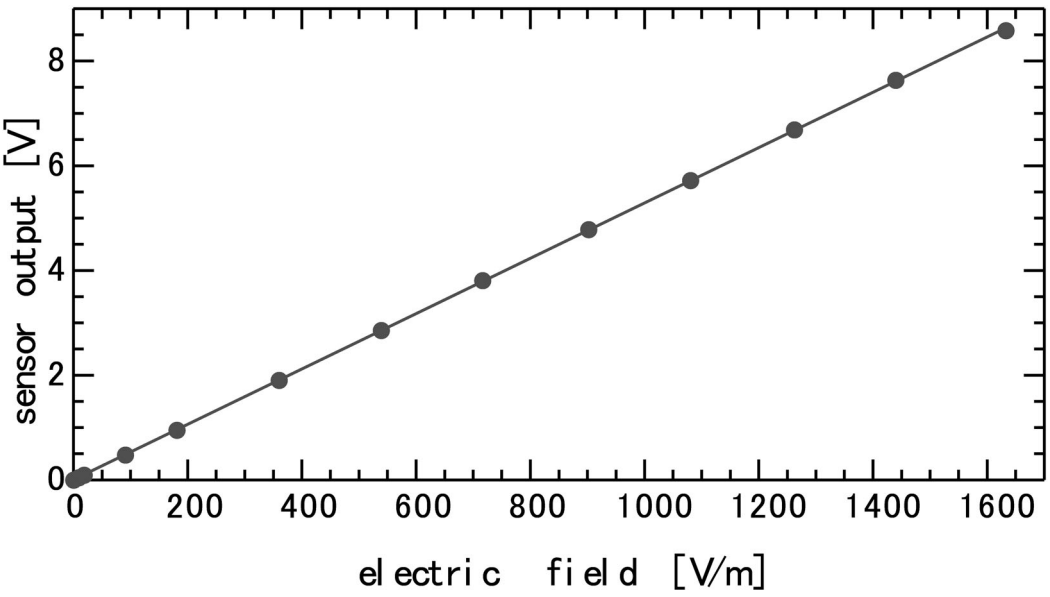

Figure 4.12: Plots of sensor output at various intensity of electric field. Light intensity is 7dBm and adopted electric field frequency is 100kHz. Sensor output increases proportionally to intensity of electric field. To change light intensity, the tangent of sensor output linear function is varied.

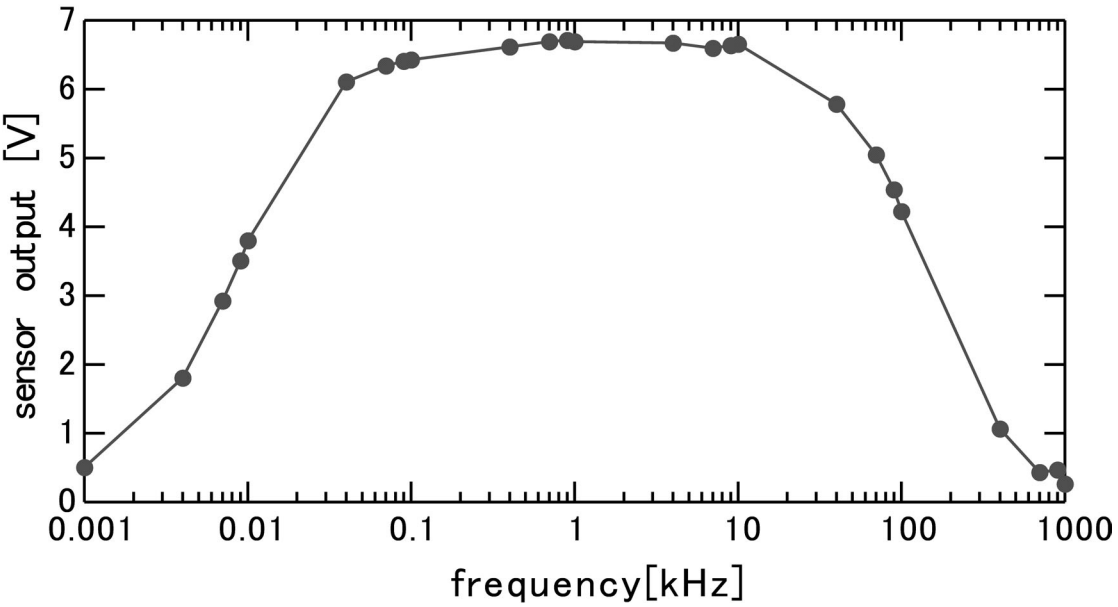

Figure 4.13: Frequency characteristic of Pockels sensor (low frequency side). Sensor output is stable between 50Hz and 100kHz. The limit of lower frequency is determined by Pockels crystal characteristic and that of higher frequency is determined by the electric circuit of light intensity detector.

Electric field induces optical phase shift between two optical paths and this shift causes interference at the output path and varies intensity.

Fig.4.8 shows configuration of Pockels sensor. ASE laser is used as a light source and laser beam is transmitted through a Polarization-maintain optical fiber. Laser enters $LiNbO_3$ modulator (probe part) and output light is converted into electronic signal at Light intensity detector. Fig.4.9 shows photograph of probe part. The size of probe is $\phi 6 \times 30mm$. The tip antenna in Fig.4.9 is to measure electric fields of radial direction.

Although Pockels sensor can be measured with frequency response from 6Hz to 2GHz, for stabilizing sensor output light detector is divided low frequency side (6∼100kHz) from high frequency side (100k∼100MHz). In this experiment, we used low frequency side only.

We introduce characteristics of Pockels sensor. To examine sensor characteristics, we measure an electric field which is applied by a pair of metal plates (Fig.4.10). Plates size is 30cm×30cm and the distance between two plates is 10cm. The hole with a diameter of 10mm is knocked at center of one of plates and we set sensor in electric field at this hole.

Fig.4.11 is the plots of sensor output normalized by maximum at various angles between Pockels sensor and electric field. To show this figure, Pockels sensor has good directional characteristic.

Fig.4.12 shows output voltage versus electric field intensity when the light intensity was 7dBm and the electric field frequency is 100kHz. Sensor output increases proportionally to the intensity of electric field. To change light intensity, the tangent of sensor output linear function is varied.

Sensor frequency response of low frequency side is shown in Fig.4.13. Sensor output was almost constant between 50∼100kHz. The limit of higher frequency is determined by the electric circuit of light intensity detector. Although an Pockels crystal can respond above 6Hz, the signal below 50Hz is cut to avoid electrostatic noise.

4.2 Electric field structures in plasmas

In this section, Pockels sensor and emissive probe measured simultaneously. IC electrode was biased among 0.7 sec.

4.2.1 pure electron plasma

Electrons were injected at R=46cm. V_ic was zero potential (chamber potential). Fig.4.14 shows the typical electron orbit which was injected at R=46cm and V_{acc} = 500V. The trajectory of electron beam is transit around IC electrode.

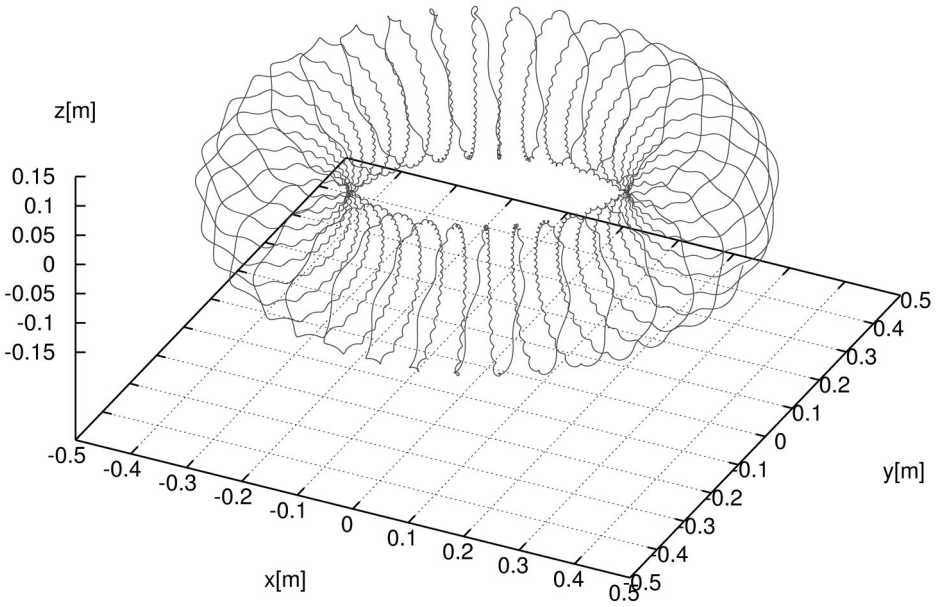

Figure 4.14: Electron orbit injected at R=46cm. The trajectory of electron beam is transit around IC electrode.

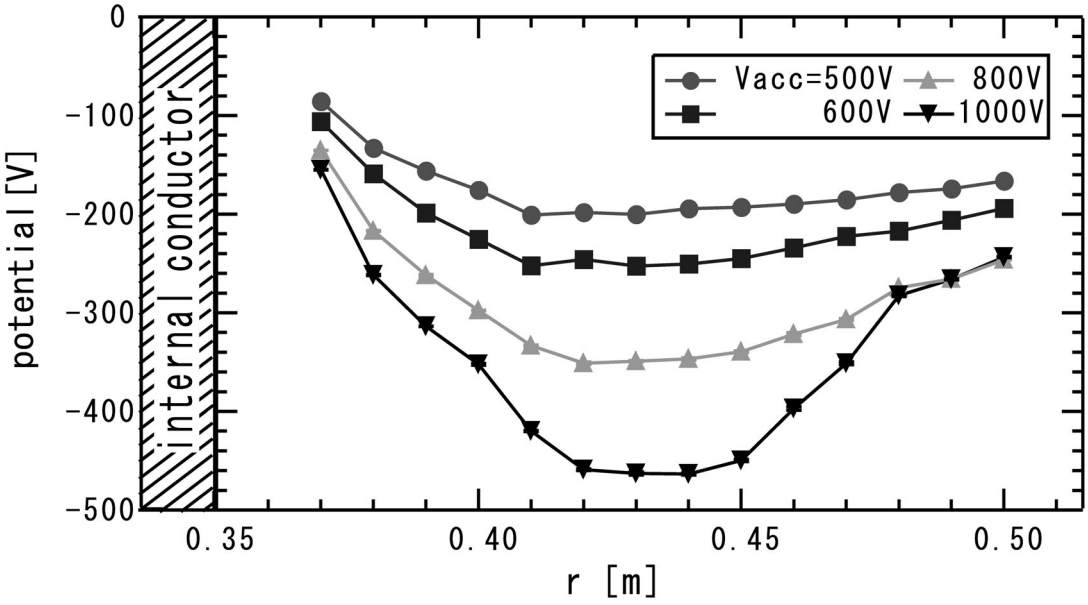

Figure 4.15: Radial potential profiles in pure electron plasma measured by emissive probe.

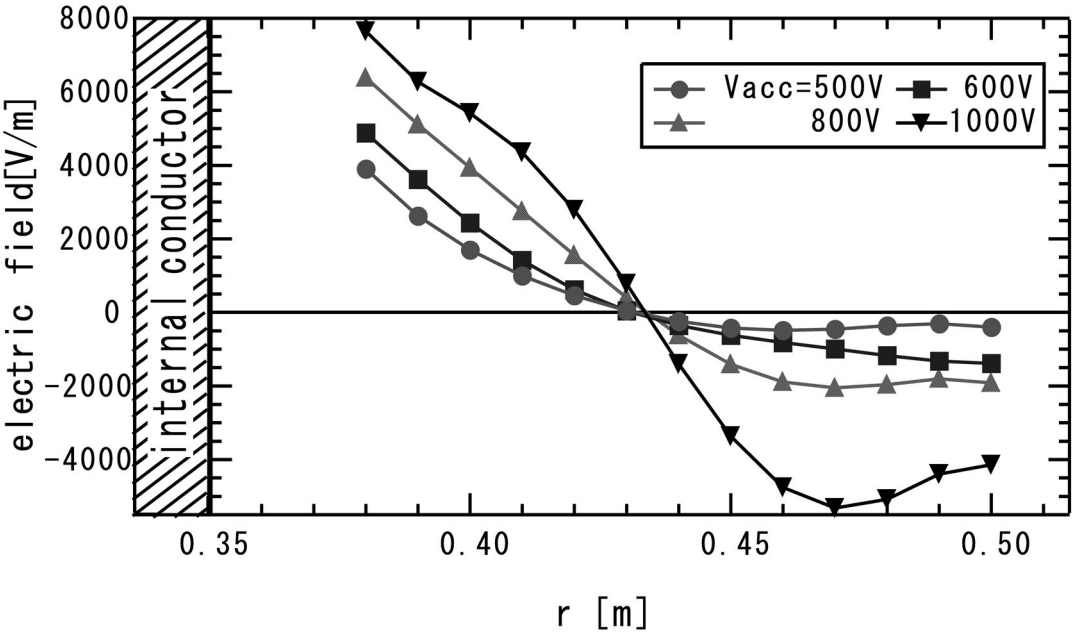

Figure 4.16: Radial electric field profiles in pure electron plasma measured by Pockels sensor and emissive probe.

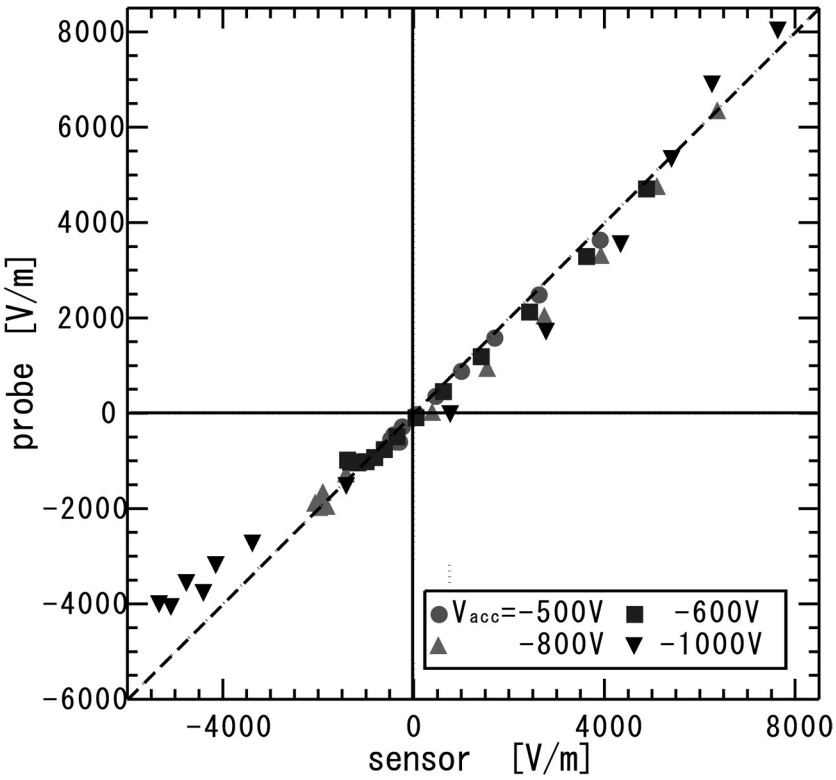

Figure 4.17: Comparing measurement result of Pockels sensor and emissive probe in pure electron plasma.

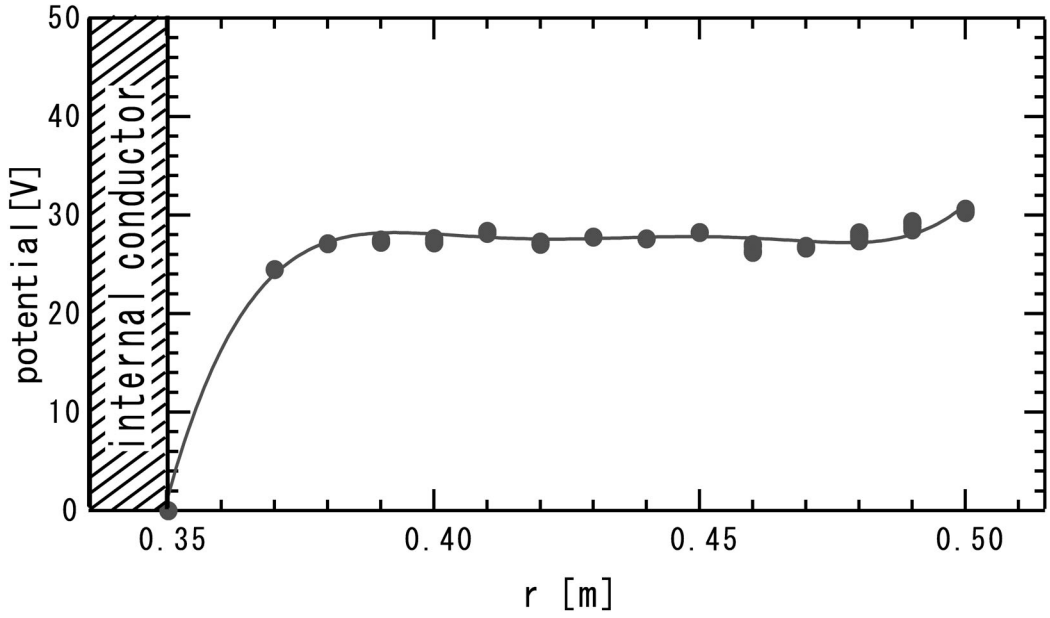

Figure 4.18: Radial potential profiles in neutral plasma measured by emissive probe.

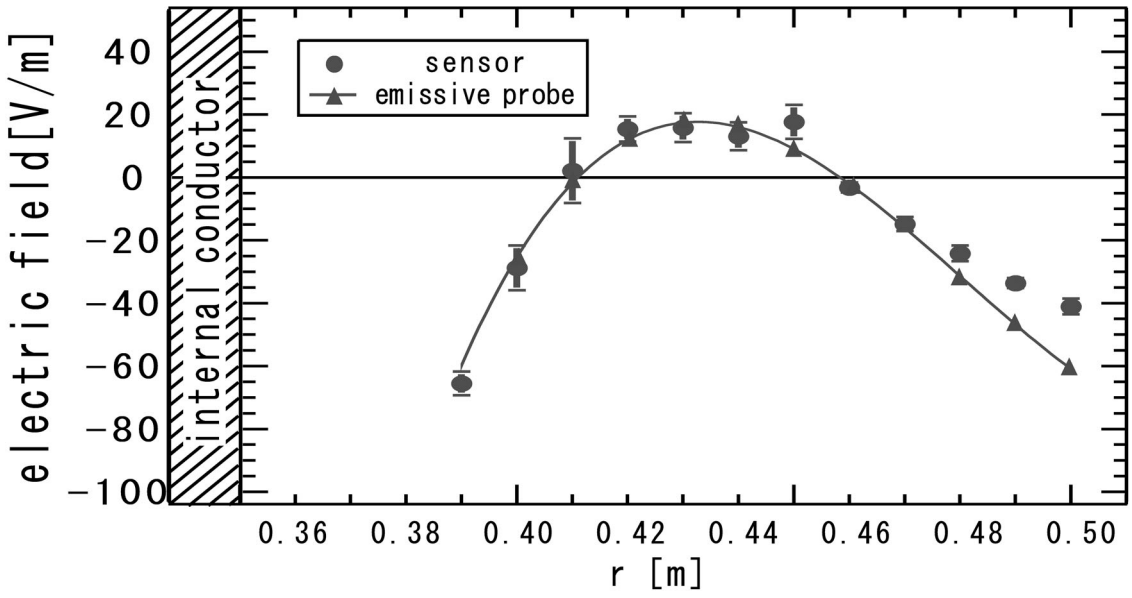

Figure 4.19: Radial electric field profiles in neutral plasma measured by Pockels sensor and emissive probe.

Fig.4.15 shows radial potential profiles in pure electron plasmas with emissive probe. The electric field structures are shown in Fig.4.16. It was measured that there was strong electric field in the vicinity of the center of electrons confinement.

Fig.4.17 shows the comparison measurement results with Pockels sensor and emissive probe. We observed that Pockels sensor measurements well accorded with emissive probe measurements within 15 % error.

4.2.2 neutral plasma

Fig.4.18 and 4.19 show radial potential profiles and radial electric field structures in neutral plasma respectively. There was scarcely existence of internal electric field.

We compared two measurement results shown in fig.4.20 and confirmed that two measurement results were exactly same.

4.2.3 electron injection

We injected electrons into neutral plasma. Electrons were injected at R=46cm in variation of acceleration voltage.

The potential and electric field profiles are shown in Fig.4.21 and 4.22, respectively. We could the plasma potential dropped near zero potential, however, the negative potential could not observed and internal electric field structures were almost similar to no electron injection.

Fig.4.23 shows the comparison electric field measurement results with Pockels sensor and emissive probe. Two measurement results were almost the same as heretofore.

4.2.4 neutral plasma biased IC electrode

We measured radial potential and electric field profiles in the variation of V_{IC}.

Fig.4.24 shows the radial profiles of the potential with different biasing of the coil surface measured by emissive probe. When V_{IC} was positive, there hardly existed plasma around the IC and the potential dropped near coil surface. With negative biasing, the electric field was smoothly distributed across the plasma.

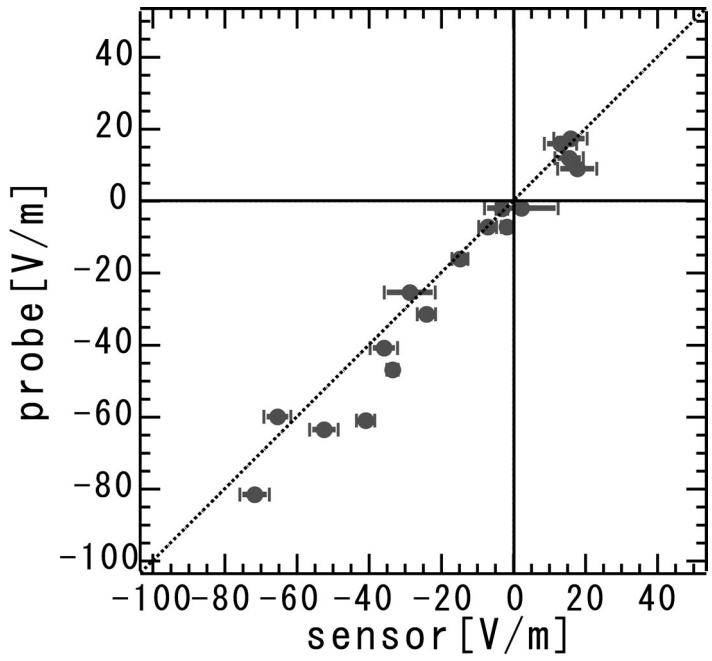

Figure 4.20: Comparing measurement result of Pockels sensor and emissive probe in neutral plasma.

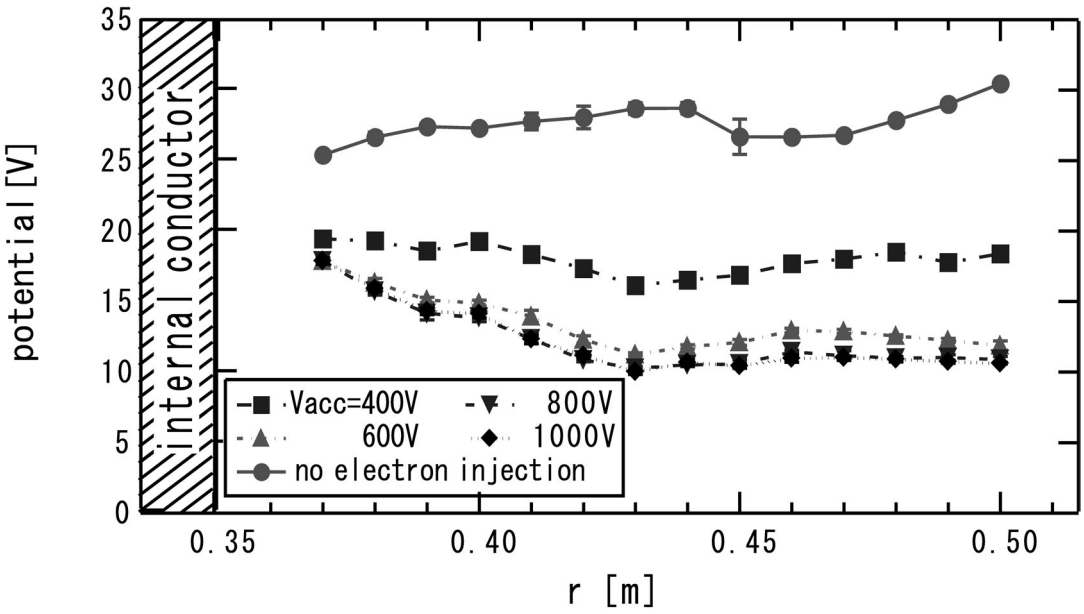

Figure 4.21: Radial potential profiles in electron injection measured by emissive probe.

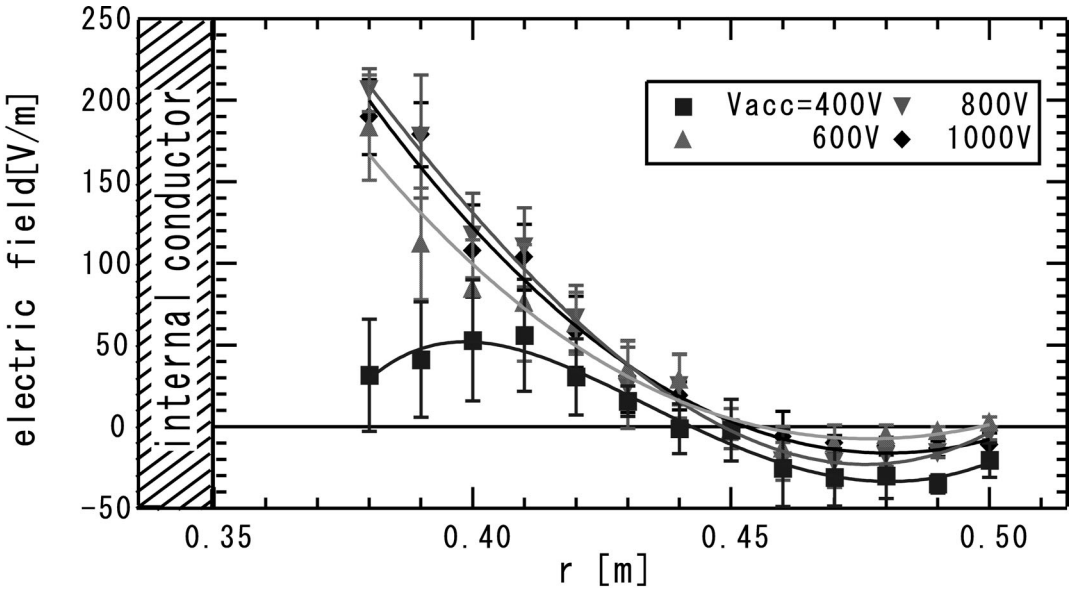

Figure 4.22: Radial electric field profiles in electron injection measured by Pockels sensor.

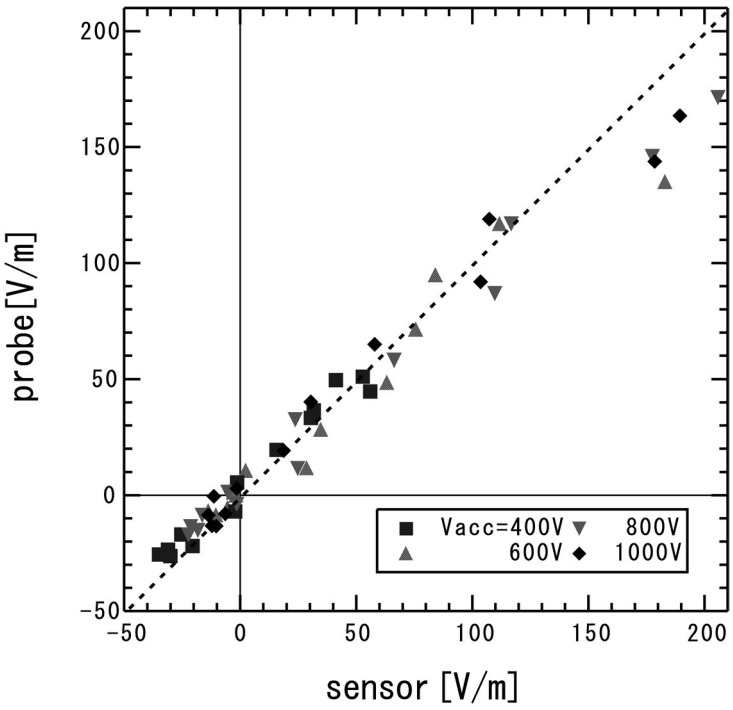

Figure 4.23: Comparing measurement result of Pockels sensor and emissive probe in electron injection.

Fig.4.25,4.26,4.27 shows radial electric field profiles with Pockels sensor and emissive probe. When the IC electrode was positively biased, electric field dropped exponentially near IC and electric field profiles at other area were almost similar to $V_{IC} = 0$. When we chose IC voltage was negative, internal electric fields were generated in the wide range of the confinement region. The observed radial electric field strengths with Pockels sensor were $\sim$6 kV/m at V_{IC}=-600 V and the corresponding $\mathbf{E} \times \mathbf{B}$ drift speed were $\sim 10^5$ m/s which were above ion sound speed. Fig.4.28,4.29,4.30 shows the comparison of electric field measurement with Pockels sensor and emissive probe. When internal electric fields were generated and strong plasma flows arose, the gap between electric field measurement results between Pockels sensor and emissive probe increased. Because two measurement results were exactly same in pure electron plasma, we thought this phenomenon caused by the effect of high speed ion. Due to collide against probe surface, ion shock wave occurred and emissive probe denotes other characteristics at weak flow plasma.

Exerting strong plasma flow on the emissive probe is discussed in next Chapter.

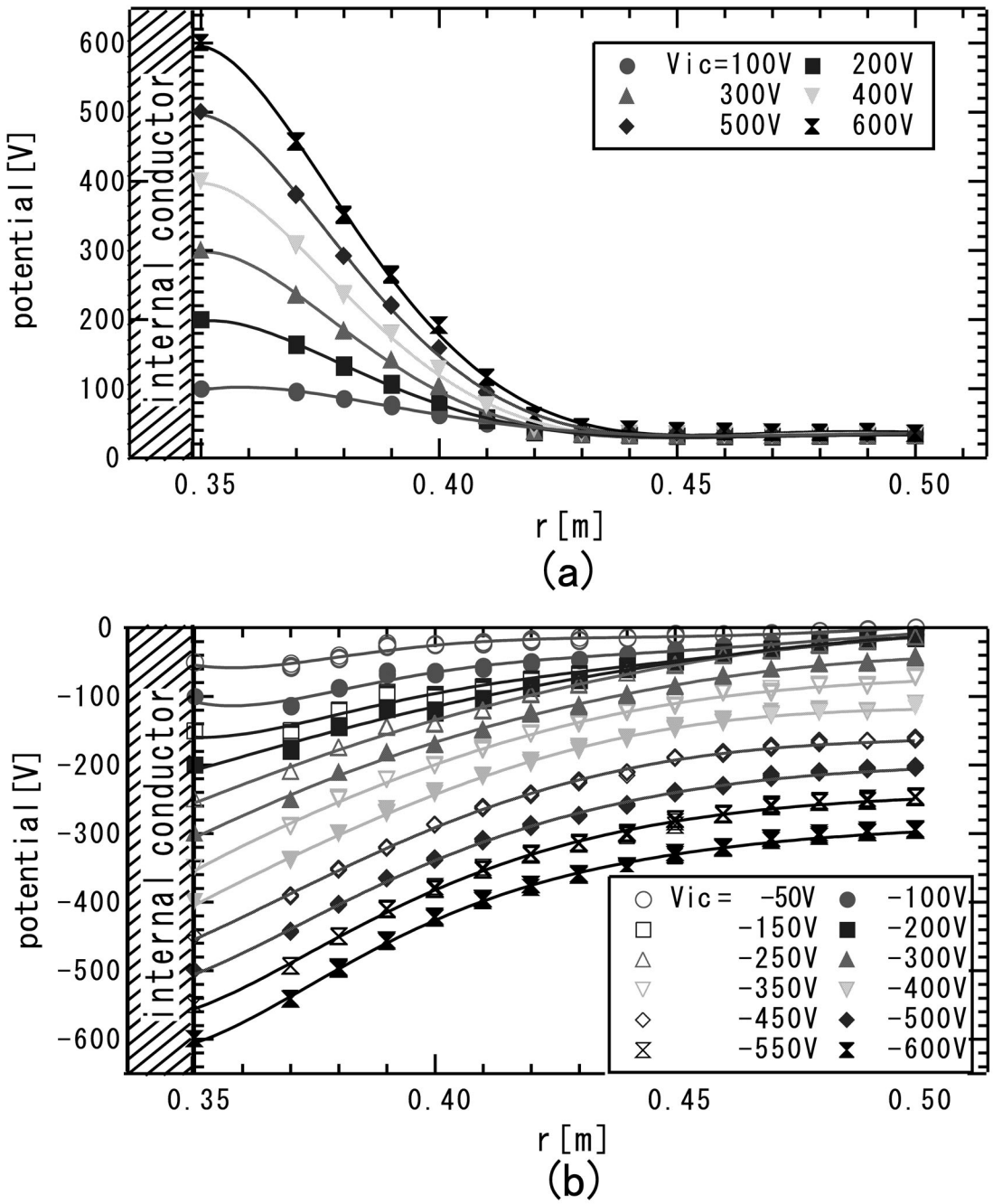

Figure 4.24: Potential structure measured with emissive probe in the variation of IC electrode biased voltage. (a) positive bias voltage and (b) negative biased voltage.

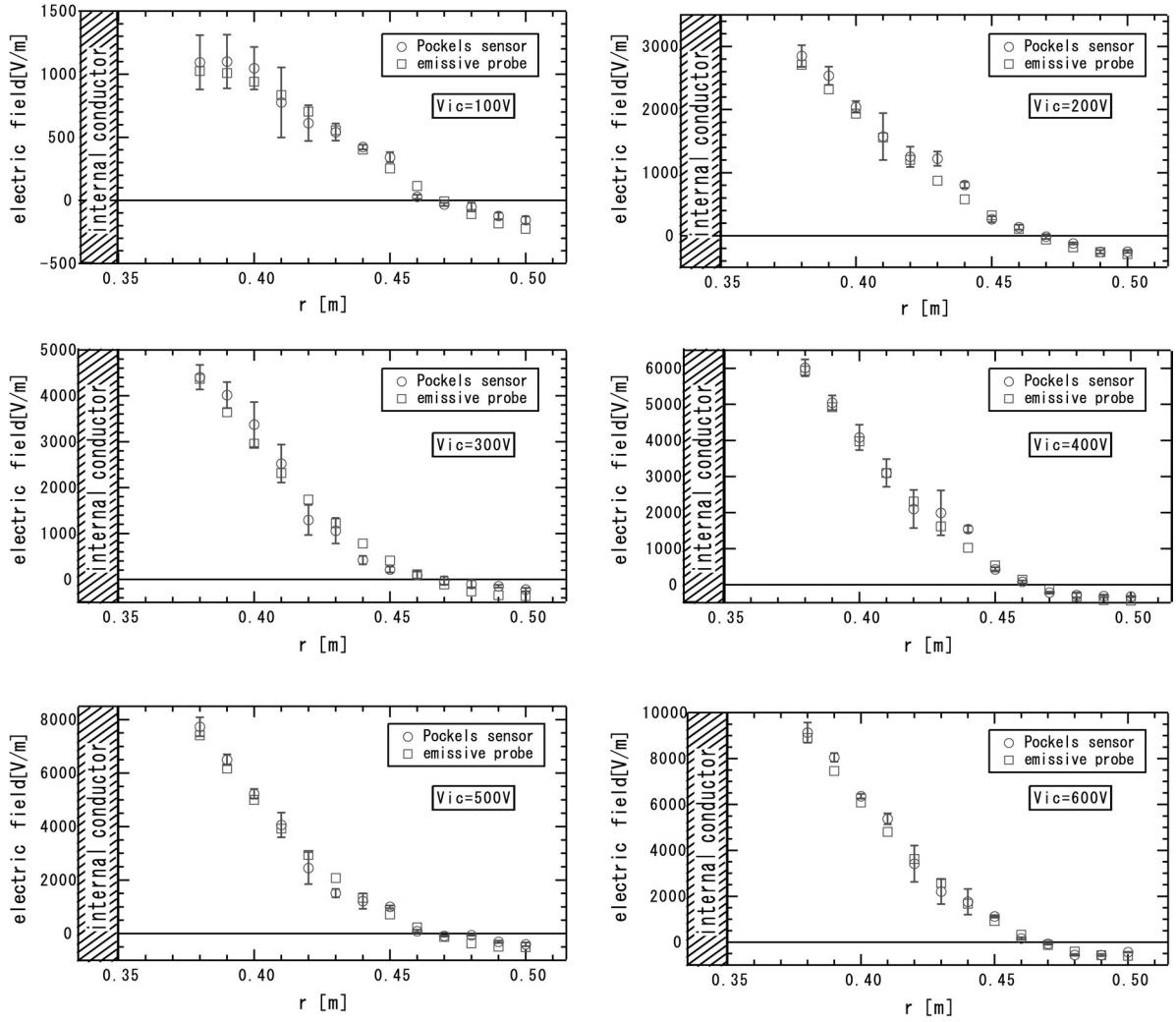

Figure 4.25: The electric field profiles result between Pockels sensor and emissive probe in electrode bias between 100V and 600V.

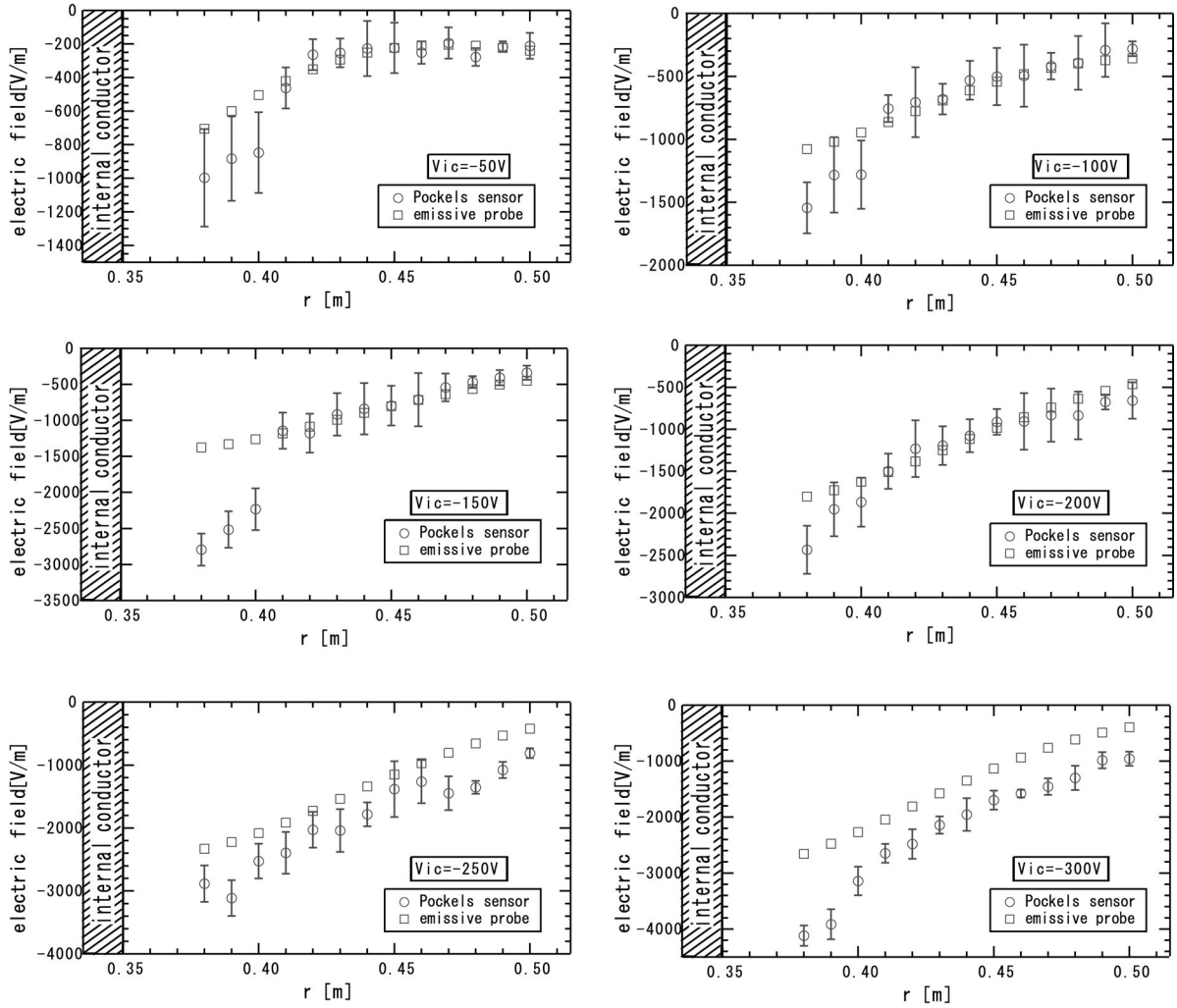

Figure 4.26: The electric field profiles result between Pockels sensor and emissive probe in electrode bias between -50V and -300V.

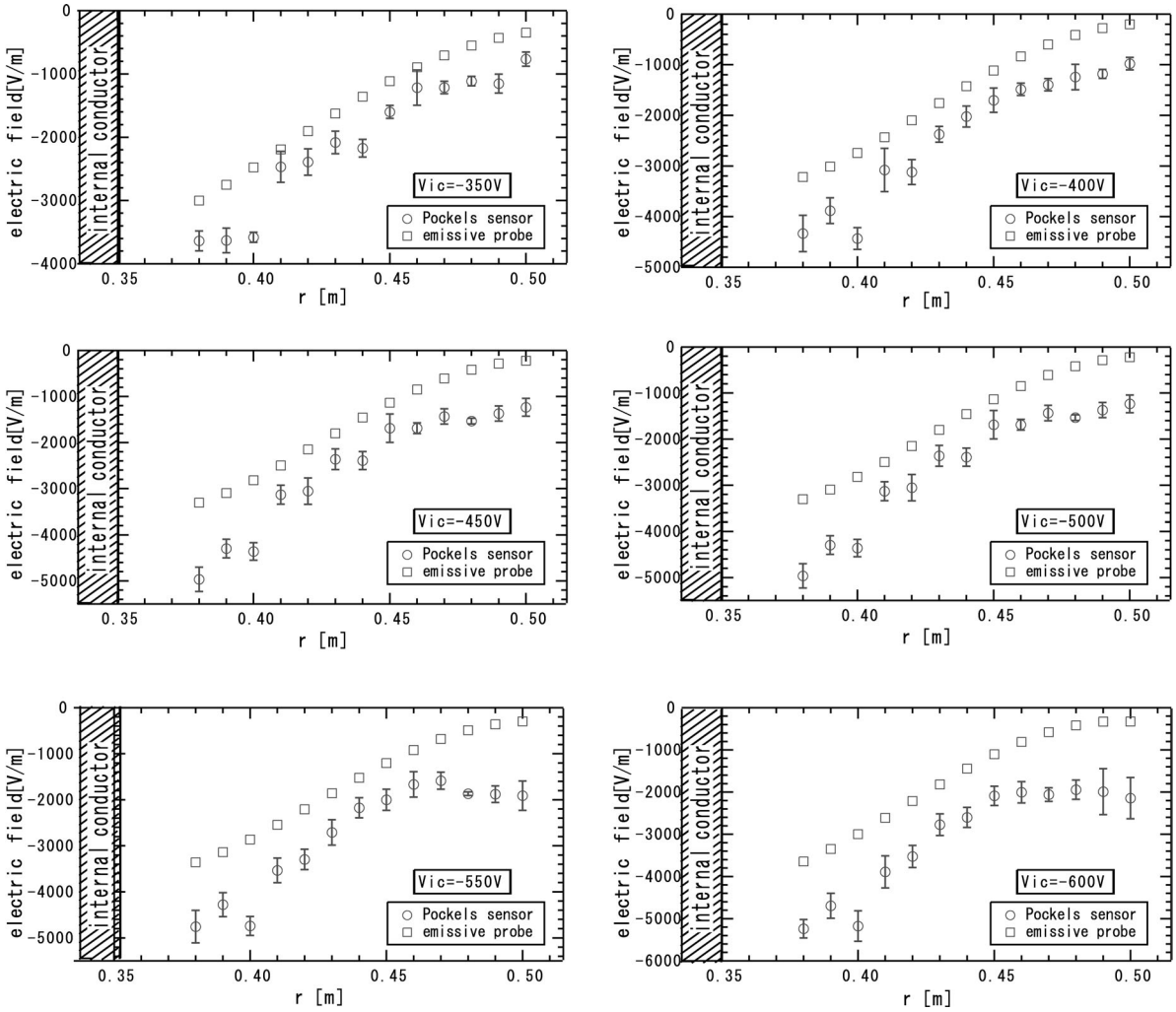

Figure 4.27: The electric field profiles result between Pockels sensor and emissive probe in electrode bias between -350V and -600V.

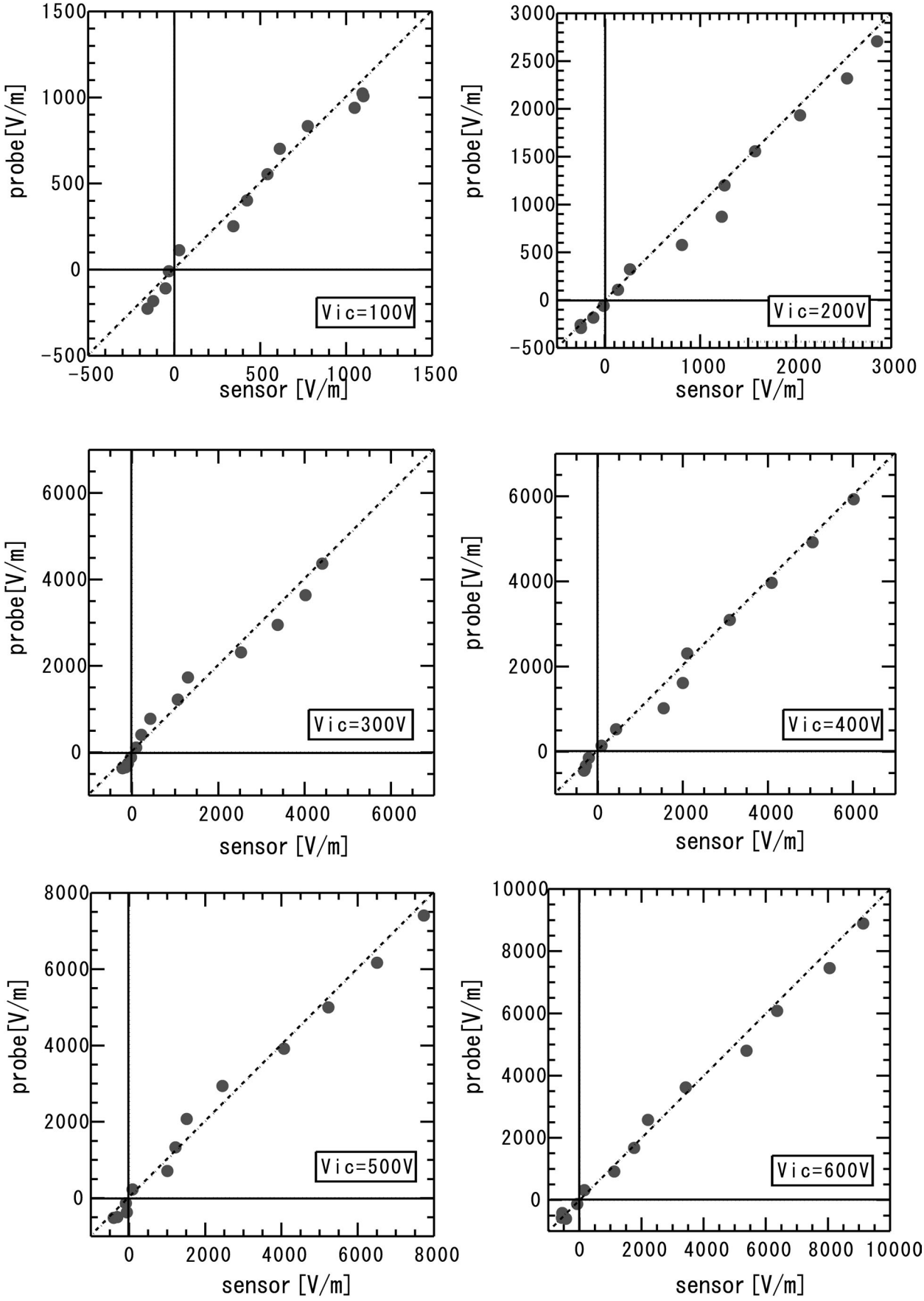

Figure 4.28: The comparison of electric field measurement with Pockels sensor and emissive probe in electrode bias between 100V and 600V.

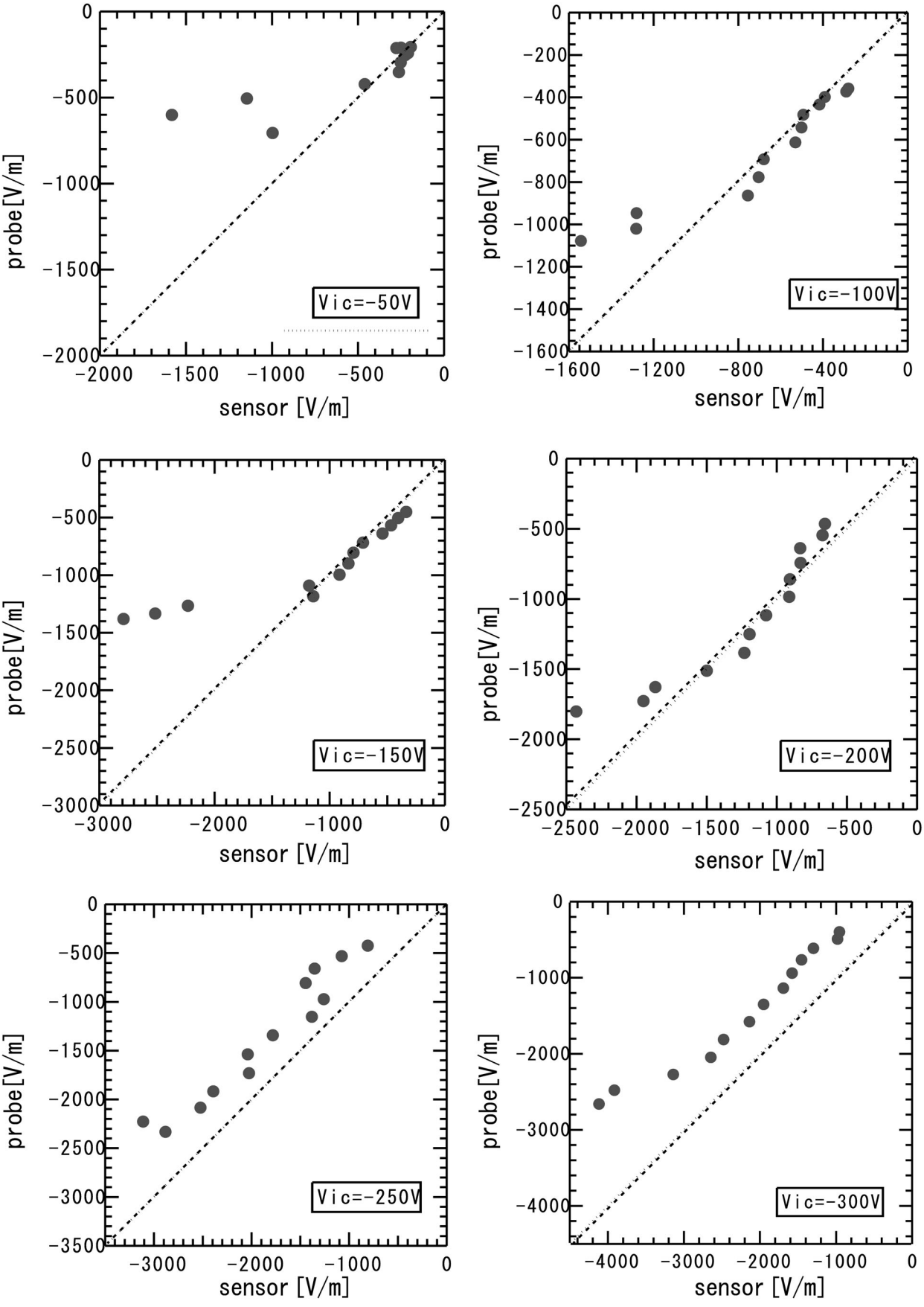

Figure 4.29: The comparison of electric field measurement with Pockels sensor and emissive probe in electrode bias between -50V and -300V.

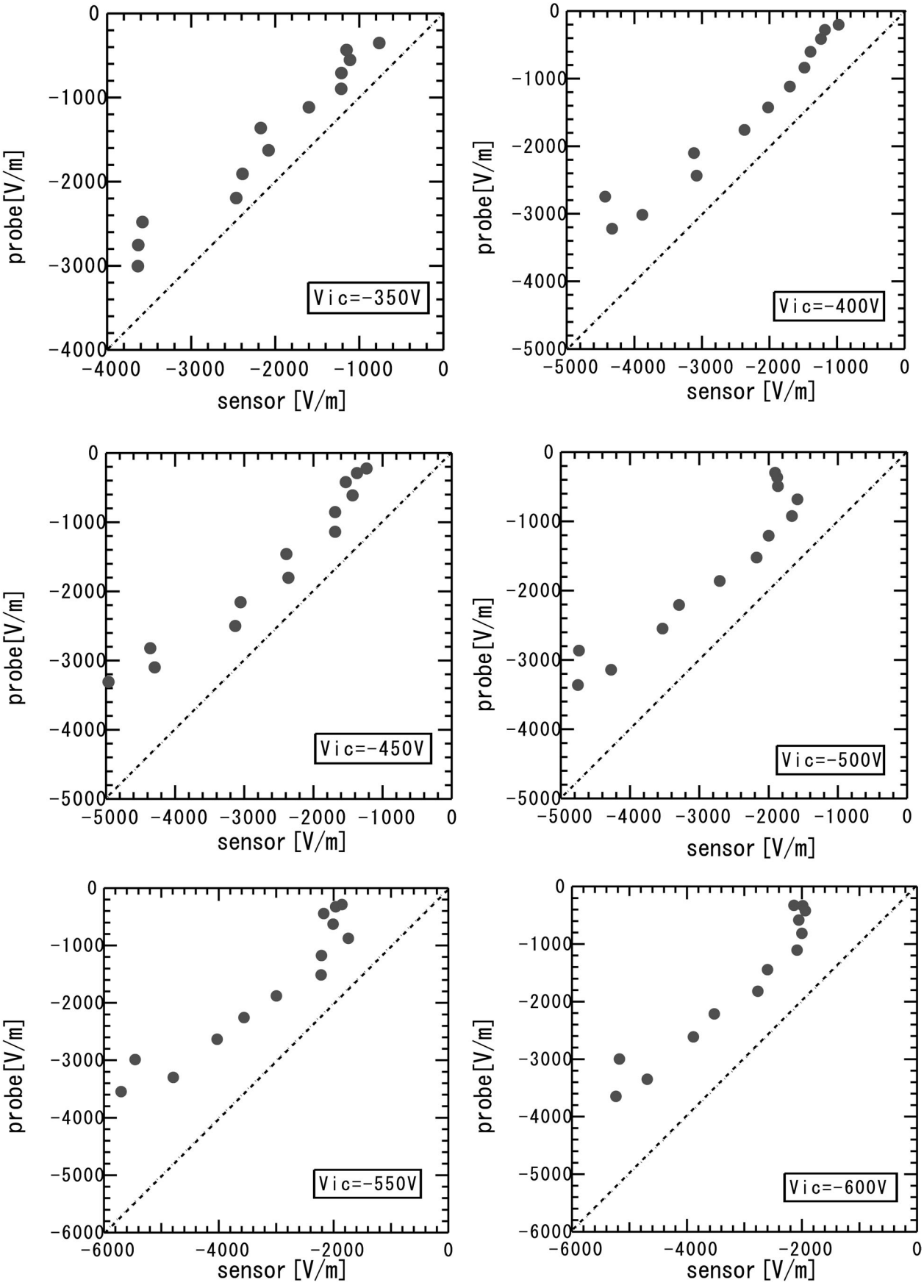

Figure 4.30: The comparison of electric field measurement with Pockels sensor and emissive probe in electrode bias between -350V and -600V.

Chapter 5

Effect of Fast Flow in Probe Measurement

Influence emissive probe exerted by high speed plasma flow (greater than ion sound speed) was experimentally studied with Pockels sensor. Investigating plasma potential with emissive probe and electric field with Pockels sensor and comparing two results, the gap raised in the measurement result when plasma flow becomes super sonic. Assuming that the result of Pockels sensor is correct, emissive probe was observed different characteristics from that in weak flow plasma . This phenomenon may cause by ion acoustic shock wave. The potential structure around probe surface was calculated and the effect of plasma flow was studied.

5.1 Experimental result

We appreciated the voltage at which cold and hot probe I-V characteristic separate as space potential with emissive probe. Plasma flow was generated by modifying electrode bias voltage on the surface of the internal coil. Pockels sensor and emissive probe were not measured simultaneously. When we measured with Pockels sensor, IC electrode was modified bias among 0.7 sec. When emissive probe I-V characteristics was measured, we biased DC voltage. But using emissive probe we checked that potential measurement results at DC biased and pulse biased were same.

Fig.5.1 shows measurements of potential with emissive probe and Pockels sensor at R=40cm. Two measurement are separate above V_{ic}=-50V. So we measure particularly at V_{ic}=-40V to -60V.

Fig.5.2 shows radial electric field profile measured by Pockels sensor and comparing potential profile with emissive probe to that with Pockels sensor is shown in fig.5.3.

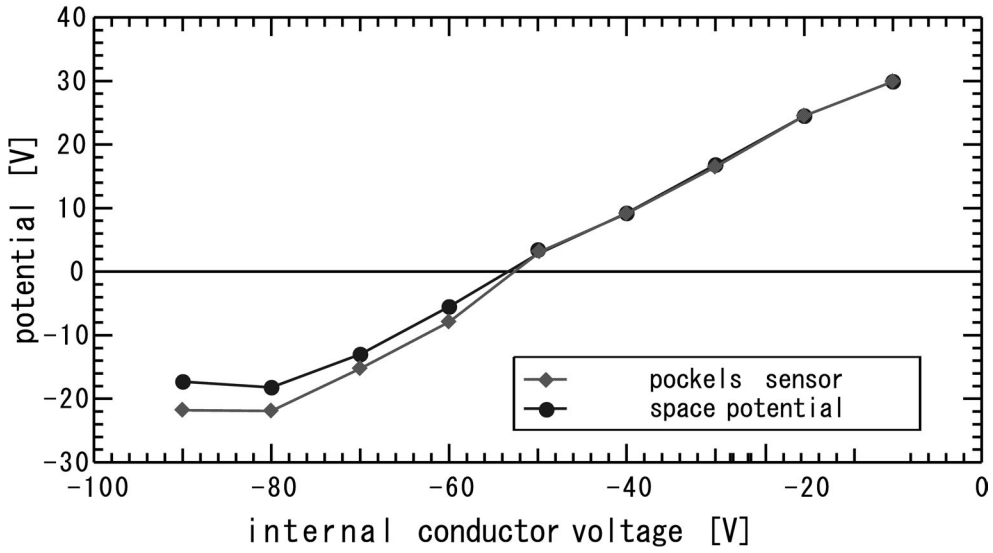

Figure 5.1: Measurements of potential with emissive probe and Pockels sensor at R=40cm. Two measurement results were separated above -50V.

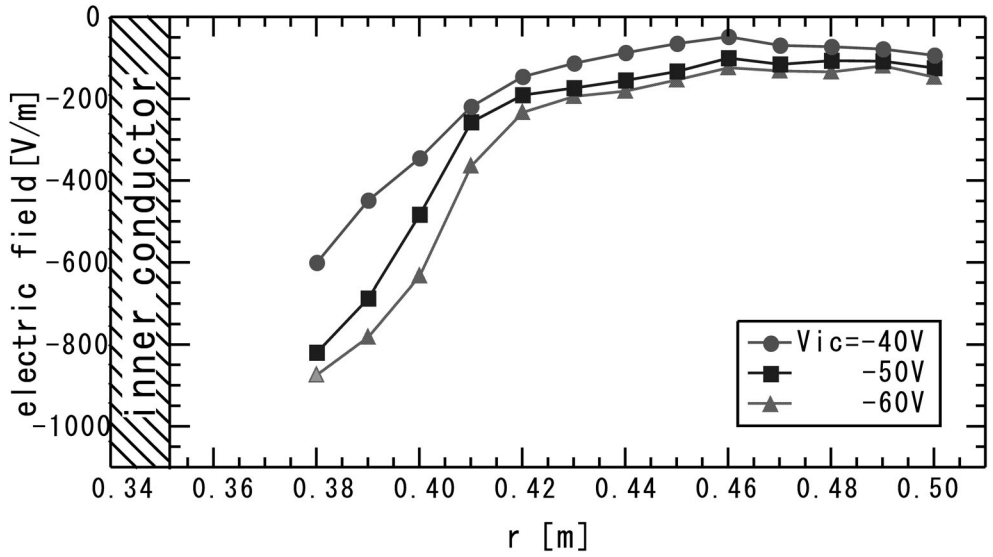

Figure 5.2: Radial electric field profile with Pockels sensor at V_{ic}=-40V to -60V. Electric field is hardly generated outside from R=41cm.

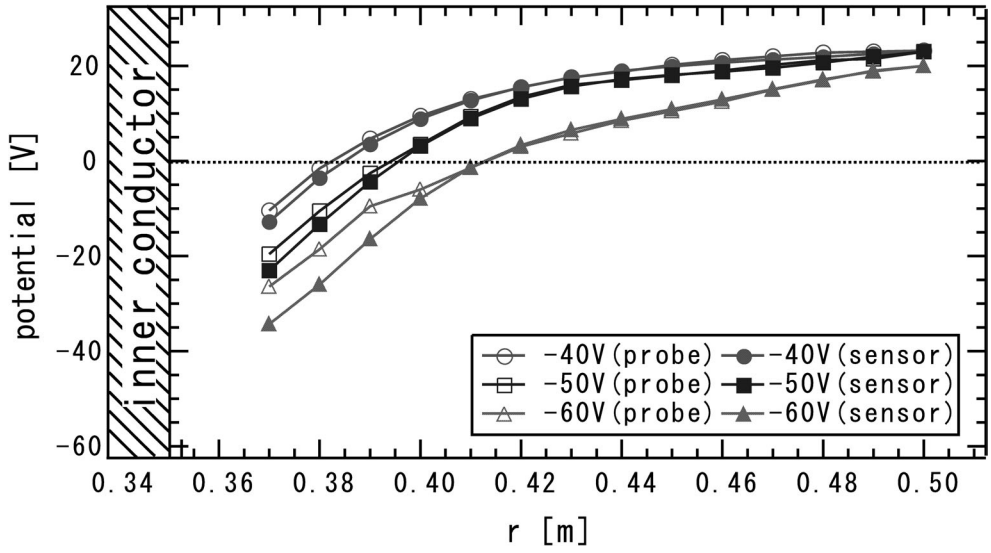

Figure 5.3: Schematic of potential measurements with emissive probe and Pockels sensor.

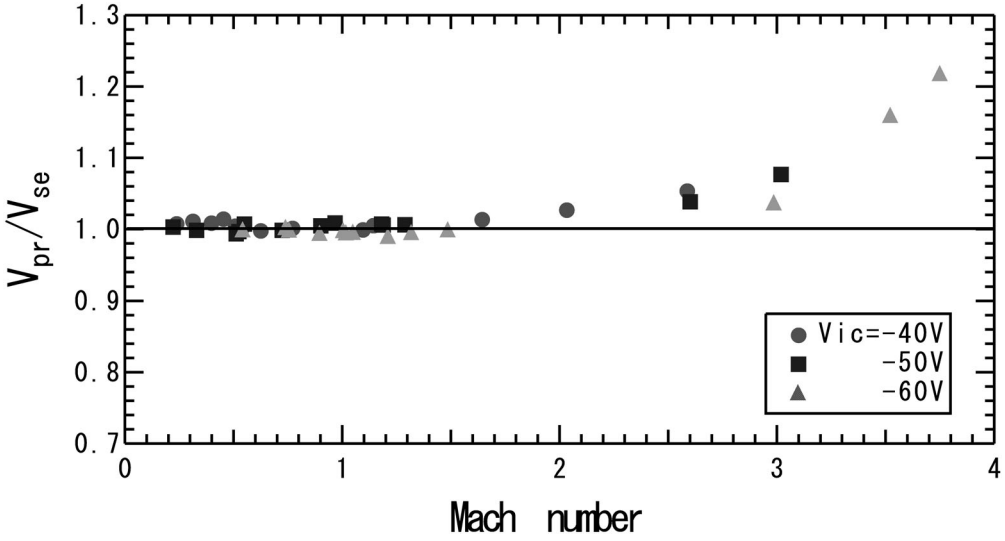

Figure 5.4: Comparison of potential measurement with emissive probe (V_{pr}) and Pockels sensor (V_{se}). Here V_{pr} and V_{se} are potential difference between the biased internal coil and measurement points.

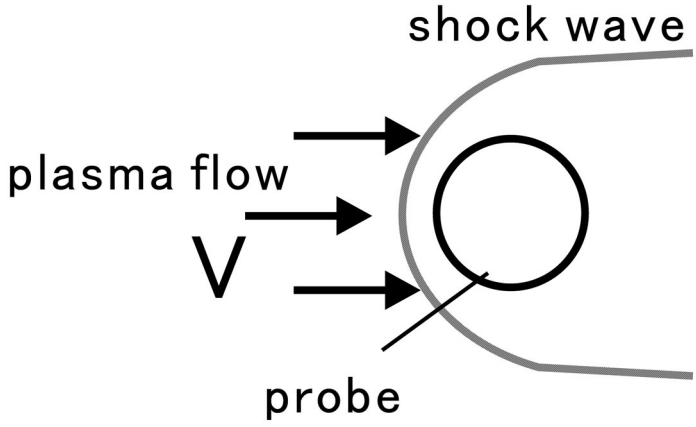

Figure 5.5: Generation ion acoustic shock wave in front of probe.

Assuming Pockels sensor was able to measure correctly, the measurement of emissive probe is under-estimate where electric field was strong.

Fig.5.4 shows comparison potential between biased internal coil and measurement points by emissive probe (V_{pr}) normalized by measurement potential by Pockels sensor (V_{se})) with Mach number calculated from $E \times B$ drift velocity which electric field is measured by Pockels sensor. The gap is appeared when Mach number is above 1.5.

Experimental results are summarized as follows. The plasma potentials measured by emissive probe were over-estimated compared with Pockels sensor measurement results in the fast flow. In pure electron plasma, two measurement results were almost the same. So we considered ions in neutral plasma gave some kind of influence on emissive probe. Measurement error caused when the plasma flow exceeded ion sound speed. So there was ion acoustic shock wave in front of emissive probe surface (fig.5.5). Therefore we calculated the potential structure around probe surface using ion acoustic shock wave model.

5.2 Calculation potential structure in ion acoustic wave

We consider simple condition that is time independent and no magnetic field, the plasma potential is determined by Poisson equation. Assuming one-dimensional hydrogen plasma model, Poisson equation can be written

$$\nabla^2 \phi = -\frac{e}{\epsilon_0} (n_i - n_e) \tag{5.1}$$

where ϕ is the potential, e is electron charge and n_i and n_e are ion, electron density respectively. For easy consideration, plasma potential far from probe is 0 and probe potential (ϕ_p) is greater than ϕ_0. Additionally, probe position is $x = 0$ and plasma flows from $x = -\infty$.
The one particle Hamiltonian for ion H_i is

$$H_i(p, x) = \frac{p^2}{2M} + e\phi(x) \tag{5.2}$$

where M is ion mass, and distribution function of ion (f_i) yield to Liouville equation

$$\frac{d}{dt} f_i + \{H_i, f_i\} = 0 \tag{5.3}$$

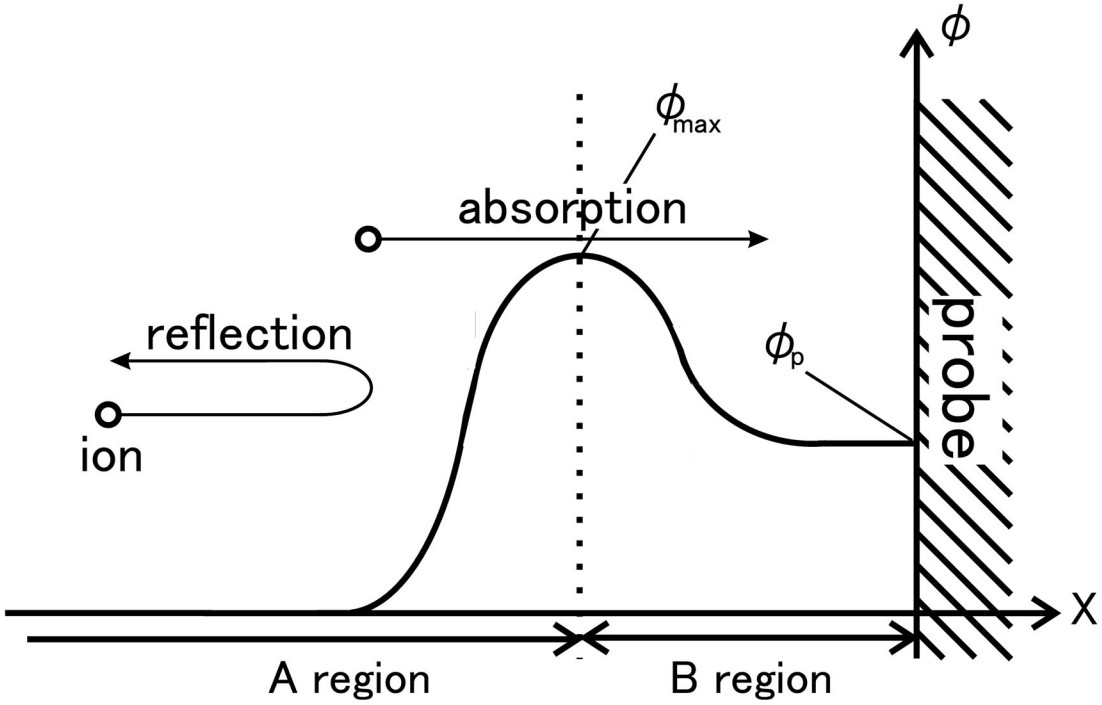

Figure 5.6: Schematic of ion particle motion. We assume particles which can reach probe are absorbed and other particles are reflected.

({ }:Poisson bracket).Supposing plasma flows at speed V and particles which can reach probe are absorbed(Fig.5.6), distribution function is given by

$$f_i = \begin{cases} \alpha \exp\left\{ -\dfrac{M}{2k_B T_i}\left(\dfrac{\sqrt{p^2+2eM\phi}}{M} - V \right)^2 \right\} & (p^2+2eM\phi \geq 0, p \geq p_{imin}) \\ \alpha \exp\left\{ -\dfrac{M}{2k_B T_i}\left(\dfrac{-\sqrt{-(p^2+2eM\phi)}}{M} - V \right)^2 \right\} & (p^2+2eM\phi < 0, p \geq p_{imin}) \\ 0 & (p < p_{imin}) \end{cases} \tag{5.4}$$

where k_B is Boltzmann constant, T_i is ion temperature, α is constant and p_{imin} is minimum momentum of ion particle which is different A region from B region and given by

$$p_{imin} = \begin{cases} -\sqrt{2eM(\phi_{max}-\phi)} & \text{(A region)} \\ \sqrt{2eM(\phi_{max}-\phi)} & \text{(B region)} \end{cases} \tag{5.5}$$

because there are only ions which can go over potential hill in B region.

In the same way, assuming all electrons absorbed by probe, electron distribution function is given by

$$f_e = \begin{cases} \alpha' \exp\left\{ -\dfrac{m}{2k_B T_e}\left(\dfrac{\sqrt{p^2-2em\phi}}{m} - V \right)^2 \right\} & (p^2-2em\phi \geq 0, p \geq 0) \\ \alpha' \exp\left\{ -\dfrac{m}{2k_B T_e}\left(\dfrac{-\sqrt{2em\phi-p-2}}{m} - V \right)^2 \right\} & (p^2-2em\phi < 0, p \geq 0) \\ 0 & (p < 0). \end{cases} \tag{5.6}$$

where α' is constant and m and T_e are electron mass and temperature, respectively. Density is given by integration of distribution function. So n_i,n_e are given by

$$n_i(x) = \int_{-\infty}^{\infty} f_i(p,x)dp. \tag{5.7}$$

$$n_e(x) = \int_{-\infty}^{\infty} f_e(p,x)dp. \tag{5.8}$$

Since plasma far from probe is neutral, we give following equation

$$n_e(-\infty) = n_i(-\infty) \equiv n_0. \tag{5.9}$$

$$\tag{5.10}$$

Normalizing by

$$x = \lambda_D \hat{x}, \quad \phi = \frac{k_B T_e}{e}\hat{\phi}, \quad p = \sqrt{M k_B T_e}\hat{p}$$

$$V = \tilde{M}\sqrt{\frac{k_B\left(T_e+\gamma T_i\right)}{M}}, \quad n_i = n_0\hat{n}_i, \quad n_e = n_0\hat{n}_e$$

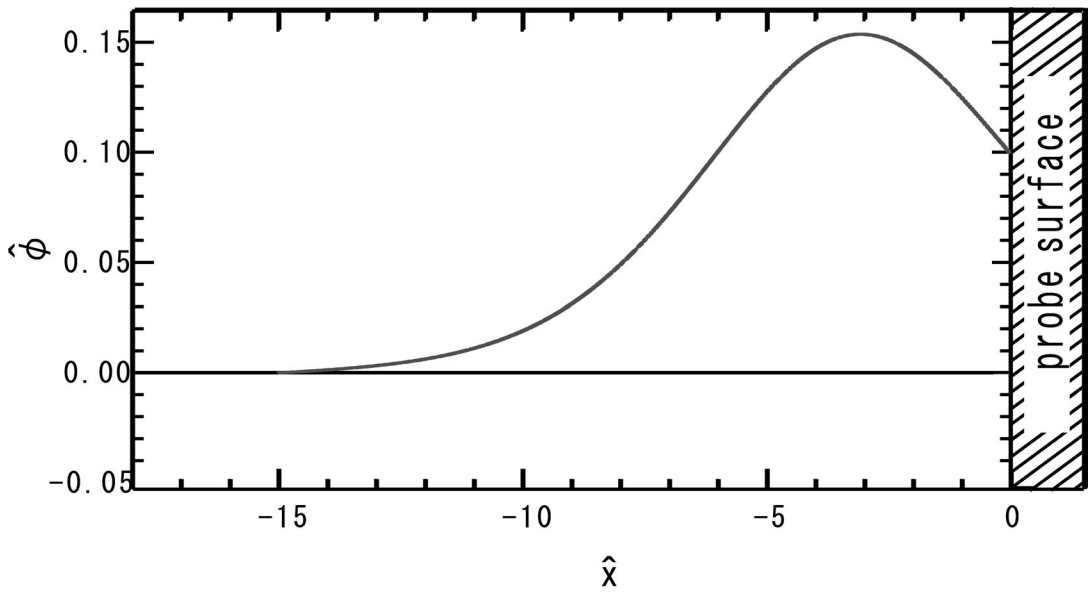

Figure 5.7: Potential structure at $\tilde{M} = 1.5$. We assume probe potential ϕ_p is 0.1 .

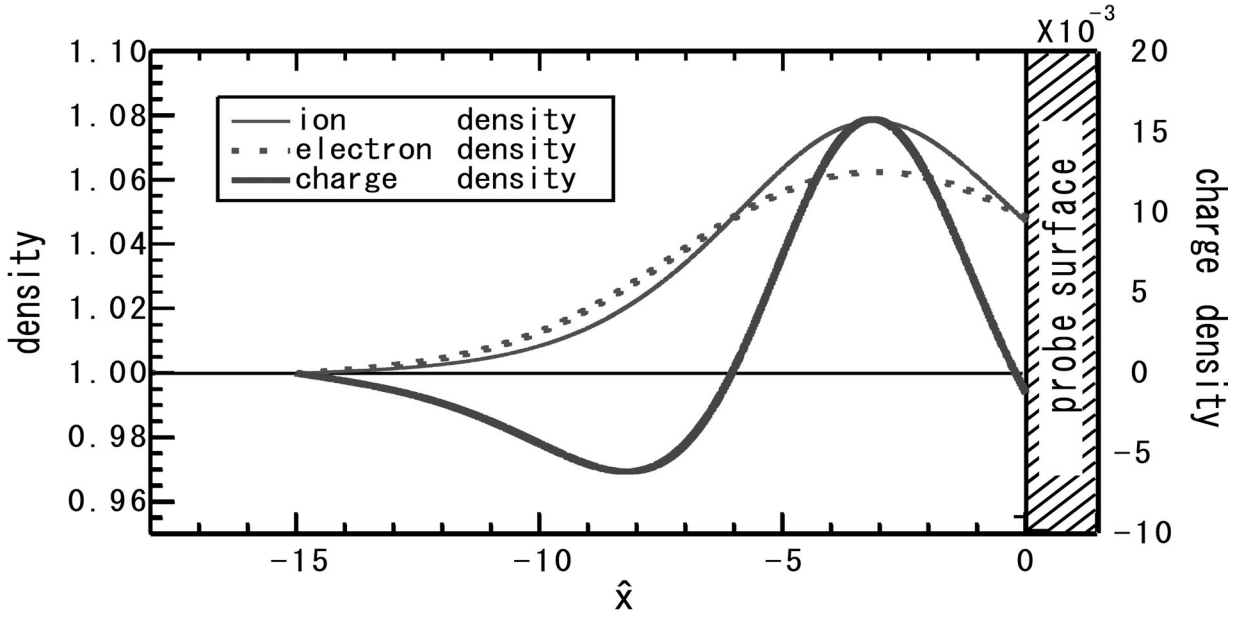

Figure 5.8: Density of ions and electron and charge density profile at $\tilde{M} = 1.5$.

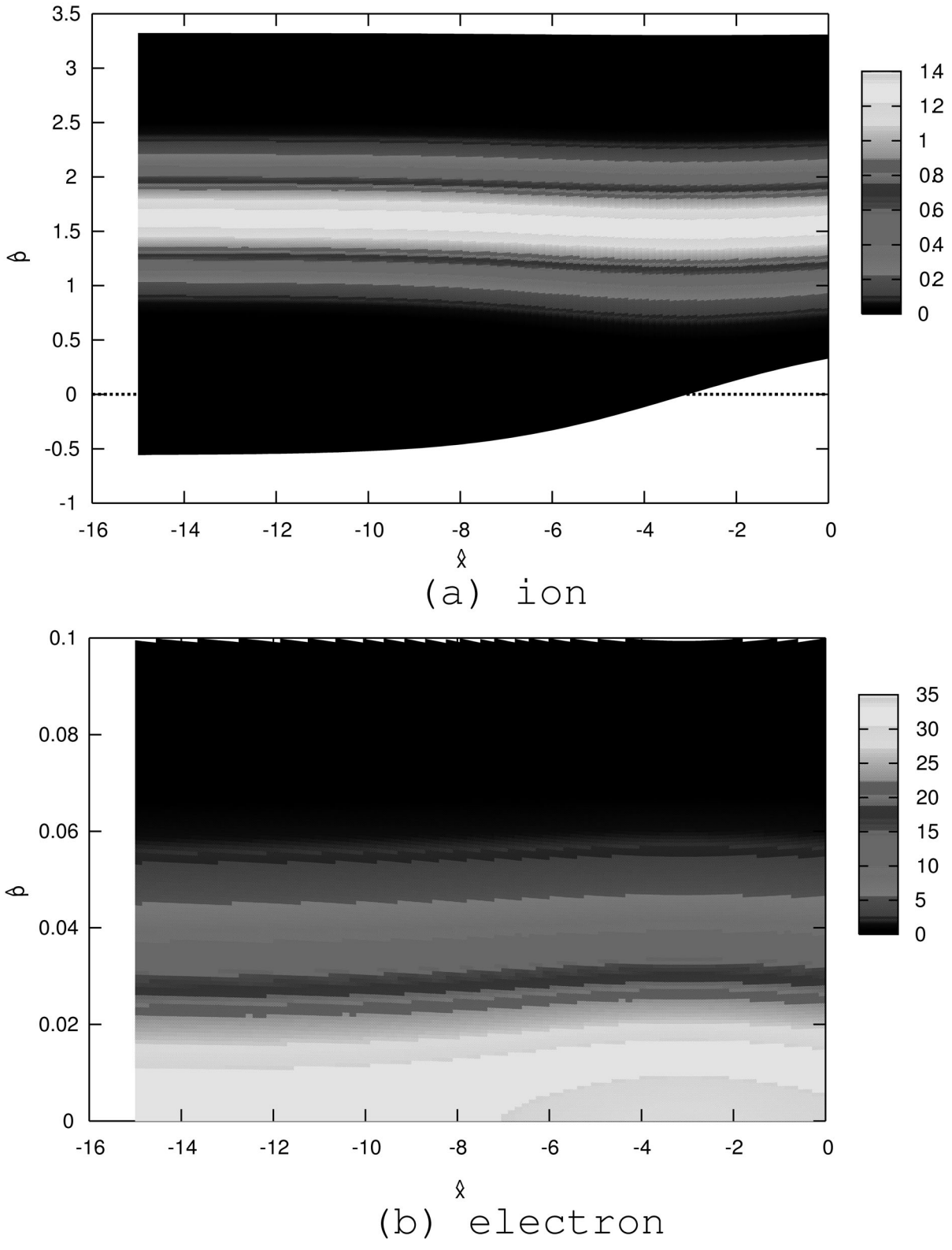

Figure 5.9: Ions and electrons distribution at $\tilde{M} = 1.5$.

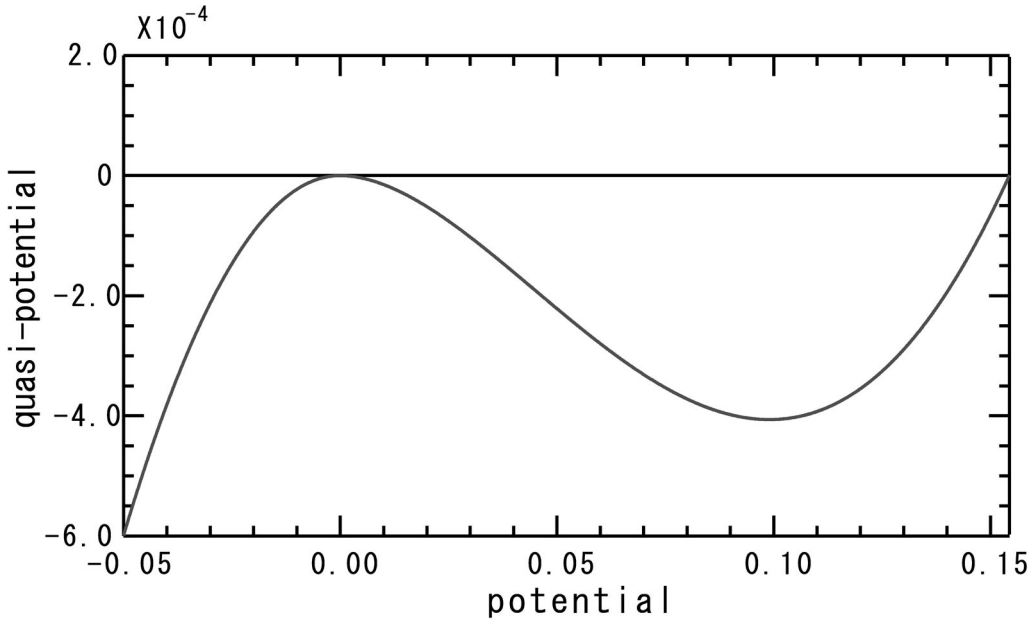

Figure 5.10: Quasi-potential structure at $\tilde{M} = 1.5$. The horizontal axis is potential $\hat{\phi}$.

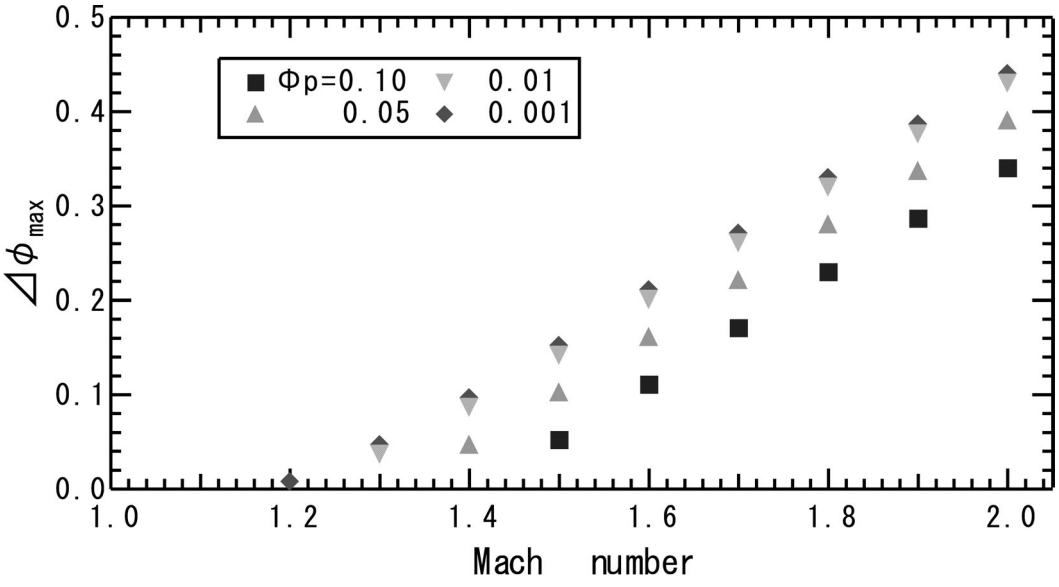

Figure 5.11: Relation between $\hat{\phi}_{max}$ and Mach number. Potential hill shows above $\tilde{M} = 1.2$

where λ_D is Debye length, $\tilde{M}$ is Mach number and γ is specific heat ratio, we can rewrite Poisson equation as

$$\frac{d^2\hat{\phi}}{d\hat{x}^2} = \hat{n_e} - \hat{n_i} \equiv -\frac{dV(\hat{\phi})}{d\hat{\phi}} \tag{5.11}$$

where

$$\hat{n_i} = \frac{\alpha\sqrt{Mk_BT_e}}{n_0}\int_{-\infty}^{\infty}\hat{f_i}d\hat{p}$$
$$\hat{n_e} = \frac{\alpha'\sqrt{Mk_BT_e}}{n_0}\int_{-\infty}^{\infty}\hat{f_e}d\hat{p}$$

$$\hat{f_i} = \begin{cases} \alpha\exp\left\{-\dfrac{T_e}{2T_i}\left(\sqrt{\hat{p}^2+2\hat{\phi}} - \tilde{M}\sqrt{1+\gamma\dfrac{T_i}{T_e}}\right)^2\right\} & (\hat{p}^2+2\hat{\phi}\geq 0, \hat{p}\geq\hat{p}_{imin}) \\ \alpha'\exp\left\{-\dfrac{T_e}{2T_i}\left(-\sqrt{-\left(\hat{p}^2+2\hat{\phi}\right)} - \tilde{M}\sqrt{1+\gamma\dfrac{T_i}{T_e}}\right)^2\right\} & (\hat{p}^2+2\hat{\phi}<0, \hat{p}\geq\hat{p}_{imin}) \\ 0 & (\hat{p}<\hat{p}_{imin}) \end{cases}$$

$$\hat{f_e} = \begin{cases} \alpha'\exp\left\{\dfrac{1}{2}\left(\sqrt{\dfrac{M}{m}\hat{p}^2-2\hat{\phi}} - \tilde{M}\sqrt{\dfrac{m}{M}\left(1+\gamma\dfrac{T_i}{T_e}\right)}\right)^2\right\} & \left(\dfrac{M}{m}\hat{p}^2-2\hat{\phi}\geq 0, \hat{p}\geq 0\right) \\ \alpha'\exp\left\{\dfrac{1}{2}\left(\sqrt{2\hat{\phi}-\dfrac{M}{m}\hat{p}^2} - \tilde{M}\sqrt{\dfrac{m}{M}\left(1+\gamma\dfrac{T_i}{T_e}\right)}\right)^2\right\} & \left(\dfrac{M}{m}\hat{p}^2-2\hat{\phi}<0, \hat{p}\geq 0\right) \\ 0 & (\hat{p}<0). \end{cases}$$

where $V(\hat{\phi})$ is quasi-potential. We considered $V(0) = 0$.

We calculated substituting Proto-RT parameter(T_e=10eV, T_i=1.0eV) and examined the relation between Mach number and $\hat{\phi}_{max}$.

Fig.5.7 shows potential structure at $\tilde{M} = 1.5$ when $\hat{\phi_p} = 0.1$. There was a potential hill near the probe surface. The density of ions and electrons and charge density profiles are shown in fig.5.8 and ions and electrons distributions are shown in fig.5.9. At the potential hill ion density was larger than electron density and charge density was positive.

To understand the solution of (5.11), we verified quasi-potential structure. Fig.5.10 shows quasi-potential structure at $\tilde{M} = 1.5$. If quasi-potential structure is well type like 5.10, the potential increases to $\hat{\phi}_{max}$ which is at $V(\hat{\phi}) = 0$ except $\hat{\phi} = 0$.

Relation between ϕ_{max} and Mach number in variation of $\hat{\phi_p}$ is shown in fig.5.11. Potential hill was generated above $\tilde{M} = 1.2$. Moreover, the stronger plasma flow, the larger potential hill becomes.

When the potential hill is generated, emissive probe considers $\hat{\phi}_{max}$ as plasma potential and although probe potential is above plasma potential, emissive probe emits electrons. Hence emissive probe I-V characteristic shifts to the direction where the voltage is larger as shown in fig.5.12.

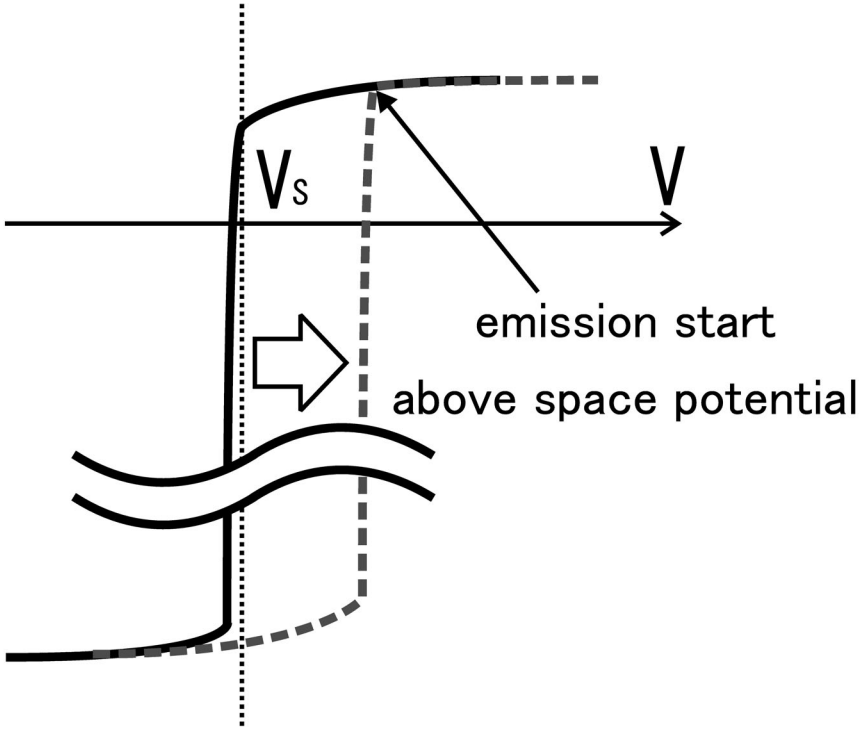

Figure 5.12: Schematic of I-V characteristic shift.

Chapter 6

Summary

In Proto-RT experiment, Pockels sensor was introduced. This sensor is an instrument measuring electric field directly using Pockels effect which is one of the electro-optical effects. Checking this measurement characteristics, the Pockels sensor has large bandwidth response.

The comparison Pockels sensor with emissive probe was studied in variety of plasmas. The sensor measurement results were similar to emissive probe measurements. In pure electron plasma, it was measured that there was strong electric field in the vicinity of the center of electrons confinement. When the surface of the internal coil was biased voltage with neutral plasma, generating internal electric field was measured with negative biasing. The toroidal flow calculated $\mathbf{E}\times\mathbf{B}$ drift velocity was above ion sound speed. Electron injection from weak magnetic field side was tested to produce internal electric field. We measured the plasma potential was reduced near zero potential, however, negative potential was not achieved and radial electric field was not generated.

Effect of high speed plasma flow on emissive probe had been studied by experiment and calculation for potential structure at ion sound wave. It is important for emissve probe characteristics to emissive electrons when probe potential was lower than space potential. In spite of well coinciding with both measurements in electron plasma, the gap of measurement result between emissive probe and Pockels sensor was generated at high speed plasma flow in neutral plasma.

We considered this gap was caused by incidence of ion shock wave and calculated potential structure on simple model. Because of increasing space potential at upstream side, emission might started at the probe potential which is higher than original space potential.

Appendix A

The Child-Langmuir Law

Fig. shows the potential structure between two infinite plane-parallel plates. The left side plate (A) emits electrons and is at zero potential, and the right side plate (B) perfectly absorbs electrons which are emitted from A and at a potential V_B.

Consider the electrons are emitted at zero velocity, the electron velocity at V potential is then

$$v = \left(\frac{2eV}{m}\right)^2 \tag{A.1}$$

where m is electron mass. So the charge density at x is given by

$$n\left(x\right) = \frac{j}{e}\left[\frac{2eV\left(x\right)}{m}\right] \tag{A.2}$$

where j is electron current density. Poisson equation becomes

$$\frac{d^2V}{dx^2} = \frac{ej}{\epsilon_0}\left(\frac{2eV}{m}\right)^{-1/2} \tag{A.3}$$

where ϵ_0 is permittivity. Multiplying by dV/dx and integrating from $x = 0$, (A.3) is written as

$$\begin{aligned}\frac{1}{2}\left(\frac{dV}{dx}\right)^2 &= \frac{ej}{\epsilon_0}\int_0^V \left(\frac{2eV}{m}\right)^{-1/2} dV \\ &= \frac{j}{\epsilon_0}\left(2meV\right)^{1/2} + \frac{1}{2}\left(\frac{dV}{dx}\right)^2\Bigg|_{x=0}.\end{aligned} \tag{A.4}$$

By space-charge-limited flow, the gradient of the potential vanishes at $x = 0$. So we have

$$V^{-1/4}dV = \left(\frac{2j}{\epsilon_0}\right)^{1/2}\left(2me\right)^{1/4}dx. \tag{A.5}$$

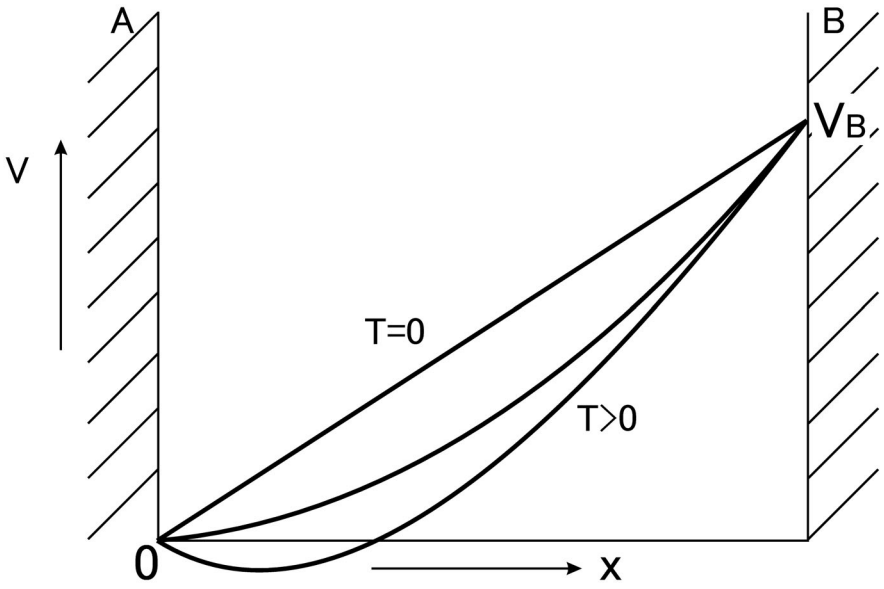

Figure A.1: Schematic of the potential distribution between two planes. Electrons are emitted from the A plane and absorbed by B plane.

Integrating from $x = 0$ to $x = d$, the electron current density is given by

$$j = \left(\frac{2}{me}\right)^{1/2} \frac{4}{9d^2} \epsilon_0 V_B^{3/2} \tag{A.6}$$

which is the Child-Langmuir $\frac{3}{2}$-power law for space-charge-limited current flow between two planes separated by a distance d with a potential V_B between them.

This model is assumed cold electrons (T=0). If the electrons have finite velocities when they are emitted (T¿0), their inertia allows them to leave the surface A even when no electric field is present. This has the effect of depressing the potential below zero and building up a field which opposes the emission of electrons. In the case of a Maxwellian distribution of emitted electrons, the potential distribution can be found by integrating over the initial distribution of temperature kT. To first order in $\eta^{-1/2}$ where $\eta = eV/kT$, Langmuir finds for the space-charge-limited current

$$j = \left(\frac{2}{me}\right)^{1/2} \frac{4\epsilon_0}{9} \frac{(V - V_m)^{3/2}}{(d - x_m)^2} \left(1 + \frac{2.66}{\sqrt{\eta}}\right) \tag{A.7}$$

where V_m is minimum potential at $x = x_m$.

Appendix B

Pockels Effect

Some kind of crystals have the behavior that the refractive index changes when an electric field is applied. This feature is electro-optical effect and these crystals are called electro-optical crystal.

The refractive indexes of the electro-optical crystals are dependent on the directions of crystal axes (anisotropic medium).

The relation between the electric displacement $\mathbf{D}$ and the electric field $\mathbf{E}$ in anisotropic medium is generally written by

$$\begin{pmatrix} D_x \\ D_y \\ D_z \end{pmatrix} = \epsilon \cdot \mathbf{E} = \begin{pmatrix} \epsilon_{11} & \epsilon_{12} & \epsilon_{13} \\ \epsilon_{21} & \epsilon_{22} & \epsilon_{23} \\ \epsilon_{31} & \epsilon_{32} & \epsilon_{33} \end{pmatrix} \begin{pmatrix} E_x \\ E_y \\ E_z \end{pmatrix} \tag{B.1}$$

where ϵ is the dielectric tensor. In lossless (reversible) medium, the dielectric tensor can be expressed as symmetric tensor. This tensor can be diagonalized to change the axis of symmetry

$$\begin{pmatrix} \epsilon_1 & 0 & 0 \\ 0 & \epsilon_2 & 0 \\ 0 & 0 & \epsilon_3 \end{pmatrix} \tag{B.2}$$

where $\epsilon_1, \epsilon_2, \epsilon_3$ are principal dielectric constant.

The electric energy density W is given as follows

$$W = \frac{1}{2}\mathbf{E} \cdot \mathbf{D} = \frac{1}{2}\left(\frac{D_z^2}{\epsilon_1} + \frac{D_z^2}{\epsilon_2} + \frac{D_z^2}{\epsilon_3}\right). \tag{B.3}$$

Substituting $x_1 = D_x/\sqrt{2W\epsilon_0}, x_2 = D_y/\sqrt{2W\epsilon_0}, x_3 = D_z/\sqrt{2W\epsilon_0}$ and the definition of refractive index $n_1^2 = \epsilon_1/\epsilon_0, n_2^2 = \epsilon_2/\epsilon_0, n_3^2 = \epsilon_3/\epsilon_0$, (B.3) is rewritten by the index ellipsoid as follows

$$\frac{x_1^2}{n_1^2} + \frac{x_2^2}{n_2^2} + \frac{x_3^2}{n_3^2} = a_{11}n_1^2 + a_{22}n_2^2 + a_{33}n_3^2 = 1 \tag{B.4}$$

where $a_{ii} = (1/n_i^2), (i = 1, 2, 3)$ and n_i is principal refractive index.

The crystal which two of three principal refractive indices are same are called uniaxial crystal and that has different refractive indices from each other called biaxial crystal.

When an electric field is applied, the principal axis of the index ellipsoid moves and (B.4) is expressed follow equation.

$$a_{11}x_1^2 + a_{22}x_2^2 + a_{33}x_3^2 + 2a_{23}xy + 2a_{31}yz + 2a_{12}zx = 1 \tag{B.5}$$

The variation of a_{ii} from primary principal axis Δa_i is given by

$$\Delta a_i = \Delta\left(1/n_i^2\right) = \sum \gamma_{ij}E_j + \sum R_{ijk}E_jE_k + \cdots \tag{B.6}$$

where γ_{ij} and R_{ijk} are Pockls coefficient and Kar coefficient respectively.

Pockels coefficient of each coordinate can be written by

$$\begin{pmatrix} \Delta\left(1/n_x^2\right) \\ \Delta\left(1/n_y^2\right) \\ \Delta\left(1/n_x^2\right) \\ a_{23} \\ a_{31} \\ a_{12} \end{pmatrix} = \begin{pmatrix} \gamma_{11} & \gamma_{12} & \gamma_{13} \\ \gamma_{21} & \gamma_{22} & \gamma_{23} \\ \gamma_{31} & \gamma_{32} & \gamma_{33} \\ \gamma_{41} & \gamma_{42} & \gamma_{43} \\ \gamma_{51} & \gamma_{52} & \gamma_{53} \\ \gamma_{61} & \gamma_{62} & \gamma_{63} \end{pmatrix} \begin{pmatrix} E_x \\ E_y \\ E_z \end{pmatrix}. \tag{B.7}$$

Fig.B shows example of Pockels crystals which are used generally.

We shows $LiNbO_3$ as example. This crystal is negative uniaxial crystal ($n_x = n_y = n_o, n_z = n_e$) and Pockels coefficient matrix is shown by

$$\begin{pmatrix} 0 & -\gamma_{22} & \gamma_{13} \\ 0 & \gamma_{22} & \gamma_{13} \\ 0 & 0 & \gamma_{33} \\ 0 & \gamma_{51} & 0 \\ \gamma_{51} & 0 & 0 \\ -\gamma_{22} & 0 & 0 \end{pmatrix}. \tag{B.8}$$

The crystal used as Pockels sensor had better have not only high Pockels coefficient but also low relative permittivity. Because if relative permittivity is high, the electric field in the crystal is small and sensitivity is low.

Table B.1: Pockels coefficient of electro-optical crystals

crystal	Pockels coefficient $\times 10^{-12}[m/V]$	refractive index	relative permittivity
$LiNbO_3$	γ_{33} =30.8	n_o =2.286	$\epsilon_\perp$ =43
	γ_{13} =8.6	n_e =2.200	$\epsilon_\parallel$ =28
	γ_{22} =3.4	n_o =2.237	
	γ_{51} =28	n_e =2.157	
		$(\lambda = 1\mu m)$	
$LiTaO_3$	γ_{33} =30.3	n_o =2.176	$\epsilon_\perp$ =41
	γ_{13} =7	n_e =2.180	$\epsilon_\parallel$ =43
	γ_{22} =1		
	γ_{51} =20		
$BaTaO_3$	γ_{33} =28	n_o =2.41	$\epsilon_\perp$ =2300
	γ_{13} =19	n_e =2.36	$\epsilon_\parallel$ =60
	γ_{51} =820		
		$(\lambda = 0.55\mu m)$	
GaAs	γ_{41} =1.2	n_o =3.6	ϵ =13.2
	$(\lambda = 0.9\mu m)$	$(\lambda = 0.9\mu m)$	
ZnO	γ_{33} =2.6	n_o =1.999	$\epsilon_\perp = \epsilon_\parallel$
	γ_{13} =-1.4	n_e =2.015	=8.15
ADP	γ_{41} =28	n_o =1.52	$\epsilon_\perp$ =58
$(NH_4H_2PO_4)$	γ_{63} =8.5	n_e =1.48	$\epsilon_\parallel$ =14
KDP	γ_{41} =8.6	n_o =1.51	$\epsilon_\perp$ =44
(KH_2PO_4)	γ_{63} =10.6	n_e =1.47	$\epsilon_\parallel$ =21

Acknowledgments

I and most grateful to Professor Zensho Yoshida. He gave me interesting subjects and precise advices in spite of his busy schedule. His accurate counsels always encouraged me and gave me line of investigation.

I also appreciate for Mr. Haruhiko Saito for his instruction. He taught experimental technique and helped my experiments. I could never have completed this thesis without his support.

I also acknowledge Professor Yuichi Ogawa, Professor Haruhiko Himura, Mr. Junji Morikawa and Professor Masayuki Fukao for their pointed indications.

I also appreciate for the member of experimental group of the laboratory, Mr. Hidenori Wakabayashi, Mr. Shigeo Yamakoshi, Mr. Tomonari Kurihara, Mr. Takuya Goto, Mr. Eiichi Yatsuka, Mr. Atsushi Wada and Mr. Kotaro Ohkuni. Especially, Mr. Goto gave me supports of school life and advantage discussions.

And I also appreciate for the member of theoretical group of the laboratory, Dr. Shuichi Ohsaki, Dr. Masaru Furukawa, Dr. Ryusuke Numata, Mr. Makoto Hirota, Mr. Dan Hori, Mr. Jun-ya Shiraishi and Mr. Shuhei Numazawa.

And I give thanks to Ms. Nami Tonegawa for their heartily support in daily life.

Finally, I would like to thank my family and friends for their concern and support.

Sho Watanabe

Bibliography

[1] Z. Yoshida and S. M. Mahajan, Phys. Rev. Lett.,**88** 095001 (2002)

[2] S. M. Mahajan and Z. Yoshida, Phys. Rev. Lett.,**81** 4863 (1998)

[3] S. M. Krimigis *et al.*, SCIENCE, **206** 977 (1979)

[4] F. Wagner *et al.*, Phys. Rev. Lett.,**49** 1408 (1982)

[5] S-I. Itoh and K. Itoh, Phys. Rev. Lett.,**60** 2276 (1988)

[6] S. M. Mahajan and Z. Yoshida, Phys. Plasmas.,**7** 635 (2000)

[7] R. J. Taylor *et al.*, Phys. Rev. Lett.,**63** 2365 (1989)

[8] H. Saitoh *et al.*, Phys. Rev. Lett. **92** 255005 (2004)

[9] H. Saitoh *et al.*, Phys. Plasmas. **11** 3331 (2004)

[10] T. Kobayashi, *et al.*, Rev. Sci. Instrum. **75**, 4121 (2004)

[11] R. J. Fonck, *et al.*, Phys. Rev. Lett. **49**, 737 (1982)

[12] K. Takizawa, *et al.*, Jpn. J. Appl. Phys. **41**, L1285 (2002)

[13] R. L. Stenzel, Rev. Sci. Instrum. **62** 130 (1991)

[14] Y. Lee, *et al.*, Rev. Sci. Instrum. **84** 4427 (1997)

[15] F. F. Chen, in *Plasma Diagnostic Techniques*, edited by R. H. Huddlestone and S. L. Leonard (Academic, New York, 1956).

[16] J. R. Smith, N. Hershkowitz, and P. Coakley, Rev. Sci. Instrum. **50**, 210 (1979)

[17] E. Y. Wang, T. Intrator, and N. Hershkowitz, Rev. Sci. Instrum. **56** 519 (1985)

[18] R. F. Kemp and J. M. Sellen, Jr., Rev. Sci. Instrum. **36**, 316 (1965)

[19] M. Y. Ye and S. Takamura, Phys. Plasmas. **7** 3457 (2000)

[20] T. Ichikawa *et al.*, Opt. Lett. **23 – 14** 1138 (1998)

Publications

Presentations at JPS

- **ポッケルス電界センサによるプラズマ中の電場構造の計測**
  渡邉将，森川惇二，齋藤晴彦，吉田善章，比村治彦，深尾正之
  2004 年次大会 28aWH-3.

- **高速プラズマ中の電場構造**
  渡邉将，齋藤晴彦，吉田善章，森川惇二，比村治彦
  2004 年秋季大会 15aXB-1.